Tracking hydrologic response of tile outlet terraces in agricultural systems to storm events

By

Marvin W. Stops, Jr.

Submitted to the graduate degree program in Geography and the Graduate Faculty of the University of Kansas in partial fulfillment of the requirements for the degree of Master of Science.

_____

Chair: Andrea Brookfield

_____

Sharon Billings

_____

Jay Johnson

Date Defended: 22 November 2019

The thesis committee for Marvin W. Stops, Jr. certifies that this is
the approved version of the following thesis:

Tracking hydrologic response of tile outlet terraces in agricultural systems to storm events

Chair: Andrea Brookfield

Date Approved: 19 December 2019

Abstract

Title outlet terrace (TOT) systems have been employed for the last century as a best management practice (BMP) to control surface runoff and associated erosion in agricultural fields. By altering the topography (artificial subsurface drainage and terraces), the hydrology of the landscape is also altered which affects the transformation, transport, and fate of applied fertilizer (nitrogen and phosphorus compounds) and their effect on other solute behavior. The study of storm events in agricultural fields is useful in identifying mechanisms of nutrient transport and transformation during runoff events under varying antecedent soil moisture conditions (pre-event) and varying growing conditions. Here we aim to track the hydrologic response of agroecosystems to storm events in TOTs to elucidate the relationship between hydrology and fertilizer use on chemical weathering fluxes by: 1) separating runoff into matrix, intermediate, and conduit flow using karst hydrology analytical methods; and, 2) pairing these results with measurements of water chemistry to identify mechanisms of nutrient transport and transformation. We focus on TOT's with constructed wetlands in the Upper Wakarusa watershed to characterize the water flux of storm events in agricultural fields. Stormwater samples were collected directly from tiles coming off three of these TOT agricultural fields and the receiving wetlands constructed to reduce nutrient runoff. Soil water samples were also collected from nested suction-cup lysimeters that are installed at 30, 60, and 90 cm at the ridge top and depression couplet of one terrace at each field site to quantify spatial variability in nutrient concentrations. All water samples were analyzed for total and dissolved nitrogen and phosphorus, total suspended solids, alkalinity, anions and cations. Storm resolved samples (every 30 mins during flow events) from tile outlets (influent storm water) and wetland outlets (effluent wetland water) were collected using automated water samplers. The digital recursive filter approach was used to separate quickflow and baseflow, as exponential fitting and master recession curves approaches failed to partition hydrographs into their components as the discharge did not behave linearly in log-space. Here the proportion of baseflow increased with the amount of incoming precipitation the week prior to the event. Mixing models derived from measured solutes show that Harvest Hills Middle (HHM, the smallest site) was closest to the atmospheric signature while Cain and Harvest Hills North (HHN) had signatures closer to nested lysimeters. This study suggests that higher tile densities led to lower hydrologic flashiness but greater chemodyanmic behavior, specifically addition behavior, and greater weathering fluxes. This was a surprising result as

more chemostatic behavior (i.e., invariant solute concentrations with large variations in discharge) was expected. These results demonstrate that there is likely an interactive effect between tile densities and terraces that may lead to non-linear behavior in solute generation and transport compared to just the effect of tiling alone.

Acknowledgements

First and foremost, nothing but the highest form of gratitude to Dr. Pamela L. Sullivan for her extreme patience, constructive guidance, and constant encouragement. Honestly, I would not be where I am now without the guidance and insights that Drs. Andrea Brookfield, Sharon Billings, and Jay Johnson have shared with me. And of course, I greatly appreciate the field and lab support from Morgan Okeson, Yane Tan, Katie Wipfli, and Matt Chomicky. As well as the funding provided by Kansas Water Office and Kansas Department of Health and Environment, Wetland Sampling funded by EPA Region 7 Wetland Program, Development Grant (CD97743401) and Kansas Water Research Institute (KWRI, Grant KAN0076261)

Table of Contents

1 Introduction 1
2 Study Area 4
3 Methods 6
3.1 Water sample collection 7
3.2 Filtering and water chemical analyses 8
3.3 Soil Collection and Analysis 9
3.4 Discharge Calculations 9
3.5 Hydrograph Analysis 10
3.5.1 Exponent Fitting Approach 11
3.5.2 Recursive Digital Filter 11
3.5.3 Master Recession Curve Approach 12
3.6 Mixing Model Analysis 12
3.7 Concentration Discharge (C-Q) Behavior and Weathering Fluxes 13
4 Results 14
4.1 Precipitation and Discharge 14
4.2 Baseflow separation 17
4.3 Water chemistry 19
4.3.1 Influent and Effluent 19
4.3.2 Lysimeters 21
4.4 Hydrograph Separation via End-member Mixing Models 22
4.5 Concentration discharge behavior 22
5 Discussion 25
5.1 Hydrologic behavior across agroecosystems with varying tile-terrace densities 26
5.2 Spatial connectivity and depth control solute chemistry across TOT systems 27
5.3 Greater tile-terrace densities support more chemodynamic behavior and greater weather fluxes 27
6 Conclusion 27
7 References 29
8 Appendices 34
8.1 Appendix 1: Precipitation and discharge data 34
8.2 Appendix 2: Base flow separation techniques 38
8.3 Appendix 3: Concentration Discharge Behavior 42

1 Introduction

The “great acceleration” is a term applied to the current Anthropocene epoch – a period marked by an increased rate in the cycling of carbon and nitrogen, and land use change from forest and grasslands to agriculture (Waters et al., 2016; Steffen et al., 2015). The impact of humanity’s growing population has led to an increased change in rates of: 1) land conversion (urban and agriculture systems now rival forest and grassland systems) (Foley et al., 2005), 2) atmospheric CO_2 concentrations (concentrations increasingly rise each year) (Peilke et al., 2002; Kump et al., 2000), 3) average global annual air temperatures (global average temperatures are increasing) (Alexander et al., 2006), and 4) the nitrogen and phosphorus cycle (reactive species have more than doubled in concentration since the industrial revolution (Bowes et al., 2015; Kladivko et al., 2004; Gruber and Galloway, 2001). Over this period, evidence is mounting to suggest that agriculture practices are shifting landscape processes from transformers-to-transporters (Kumar et al., 2018; Blann et al., 2009; Shilling and Helmers, 2008). Here, anthropogenic changes to the landscape have shifted the hydrologic response from a longer residence time of water-mineral interactions, “transformer-controlled system”, to those in which the water-mineral interactions have a shorter residence time. This increases the rate at which these fluxes enter receiving surface waters, becoming a “transporter-controlled system” (Kumar et al., 2018). The hydrologic impact of artificial manipulation to the land surface (e.g., tilling, berms, terraces) and subsurface drainage systems (e.g., tiles) is well established in the literature with a consensus that flow contributions from these “transporter” systems increases inputs of event water and nutrient losses (Kladivko et al., 1999). For example, master recession curves (MRC) analysis –an approach focused on understanding the behavior of the receding discharge after a storm event from tile-drained watersheds were more linear than less-tiled drained watershed, implying more homogenous flow paths in tile-drained systems (Shillings and Helmers, 2008). What remains less understood is the impact of multiple, interacting surface and subsurface manipulations on landscape hydrology and the cascading biogeochemical response. This research specifically focuses on the impact of tile-outlets-terrace (TOT) density on discharge following storm events through the use of a recession curve approach in order to understand the overall impact of altered hydrology on chemical weathering due to controlled partition of runoff water, infiltration, and soil moisture conditions.

For decades, *Tile outlets* or tile lines – subsurface drainage pipes, similar to sewer systems – and *Terraces* – constructed, horizontal areas created to divide sloping terrains by reducing slope steepness – have been two best management practices (BMPs) often used to reduce the impact of overland flow on soil erosion in agricultural environments (Wei et al., 2016) (Figures 1 & 4).

Hydrologically, these two approaches differ as tiles move the energy from overland flow into the subsurface, thus reducing erosion (Kladivko et al., 2004; Goolsby et al., 1999), while terraces slow the energy of overland flow by reducing the topographic gradient (Shilling and Helmers, 2008; Kladivko et.al., 2004). TOTs can be used in combination to further reduce surface water runoff during storm events, and further alter the hydrologic flow paths and spatial variability in soil moisture. These hydrologic alterations coupled with fertilizer applications can reorient the transformation and transport of nutrients and alter fluxes of chemical weathering; yet, the degree to which either controls chemical weathering is not well understood.

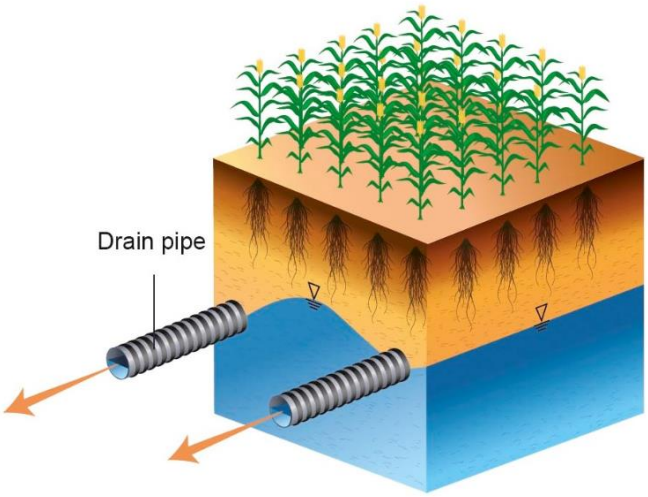

Figure 1. Tile outlets image from google depicting sub-surface drainage (tile outlets).

With much of the central USA underlain by tiles or TOTs (Blann et al., 2009) there is a need to understand how altered landscapes, subsurface hydrologic processes and their combined impact shifts the terrestrial biogeochemical processes. The analytical methods of recession curve analysis from karst aquifer flow systems provide a potential conceptual tool for understanding TOT hydrology (see Fig. 1; Shilling and Helmers, 2008a, 2008b). Here TOTs analyses can leverage that fact that karst aquifers are often characterized by a "triple permeability" (White, 2002), where subsurface water flow is evolved from the interaction of diffuse, intermediate, and conduit permeability/porosity (White, 2002; Palmer et al., 1999). Diffuse permeability is the intergranular porosity of un-fractured bedrock; intermediate permeability are mechanical joints,

joint swarms and bedding plane partings; conduit permeability are pipe-like openings that start at 1 cm (White, 2002). If a single point of outflow or discharge (Q) can be measured in a karst system, then these locations are thought to integrate various hydrologic flow paths contributing to discharge (e.g., runoff flow (conduit flow), matrix flow (diffuse flow), and intermediate flow (a mixture of both runoff and matrix flow)) that occur at different rates in time and space within a catchment (Baedke and Krothe, 2001; Tallaksen, 1995; Milanovic 1981). If TOT agriculture systems operate in an analogous manner to that of karst, the integrated signal at the outlet of a tile drain may represent all three flow regimes. Shillings and Helmers (2008) applied this same approach to tiled agriculture watersheds for three storm events and found that 66.5% of the events had two flow regimes (conduit and intermediate) and 33.5% had three flow regimes that contributed to the hydrograph response, where the contribution of three flow regimes was concomitant with a discharge response. Elevated soil moisture or heavy rainfall events could both be invoked to explain faster discharge responses.

It is important to note that in the field of hydrology, hydrograph analysis approaches such as hydrograph separation and recession curves are considered an inverse problem, as "non-unique" solutions regarding flow path contributions or aquifer properties can be derived (Rehrl and Birk, 2010). A non-unique solution can be better constrained using multiple recession curve analysis techniques and non-reactive tracers such as dye, stable isotopes, and chloride to verify the estimated parameters or contributions of flow paths to spring discharges (e.g. end member analysis; Shilling and Helmers, 2007; Christopherson and Hooper, 1992). Like karst aquifer springs, the extensively modified hydrology of TOTs possess a unique "fingerprint" of the physical and chemical processes integrated within the catchment (White, 2002; Baedke & Krothe, 2001; Palmer et al., 1999; Dreiss, 1989). Water moving through tiles may establish a similar "fingerprint" indicating solute sources generated during tile outlet discharge. Sources of solutes may arise from shifts in mineral saturation indices (Shuster and White, 1971), and contributing source waters that have distinct chemical signatures due to fertilizer inputs (Barak et al., 1997) or differences in mineral-water contact time (Gaillardet et al., 1997). For example, an increase in conduit flow might prompt mineral saturation indices to drop further below equilibrium (i.e., increased potential for mineral dissolution), or high concentrations of elements like Mg and Si might indicate greater inputs of soil or groundwater that has had longer mineral-water interaction time (Li et al., 2017). Thus, to better understand the impact of TOTs on the

hydrologic behavior of the landscape it is best to use both the recession curve, end member mixing analysis, and concentration-discharge (C-Q) relationships.

In this work, we hypothesize that a higher tile-terrace density on the landscape will result in a flashier system where large precipitation events are required to yield discharge in order to overcome lower soil moisture conditions compared to systems with low TOT density where discharge is supported by lower intensity storms. This change in behavior will yield lower chemical weathering fluxes and more invariant concentration-discharge (chemostatic) behavior from high tile-terrace density systems compared to low tile-terrace density systems (Figure 2).

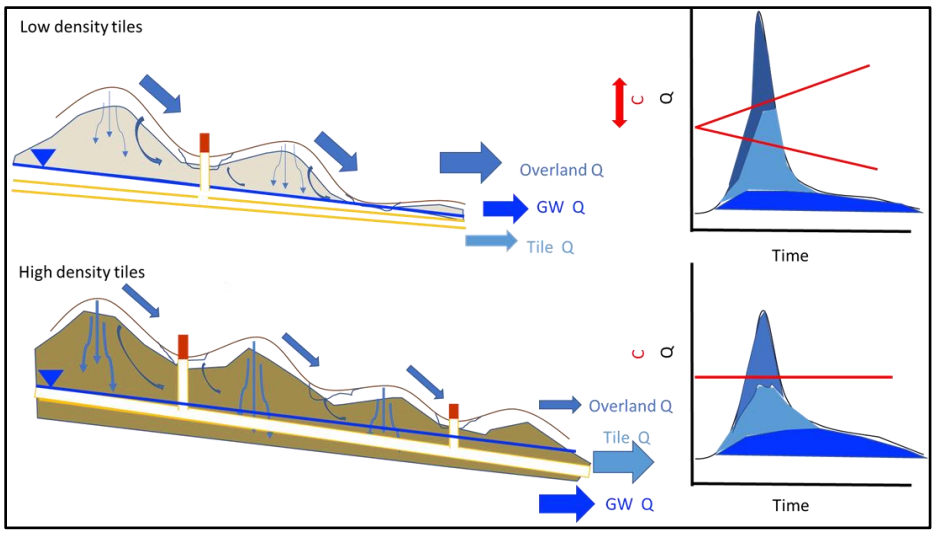

Figure 2. A schematic diagram of the proposed hypothesis. The color gradient of arrows indicate the proportion of water flow processes with representative hydrographs under each assumption. The red arrows indicate the assumptions.

2 Study Area

For this work, we compared three tile terraced cropland systems located within the Upper Wakarusa Watershed in Douglas County, KS, draining to Clinton Lake (Figure 3): Harvest Hills North (HHN; 38°59’05.5” N, 95°27’19.0” W); Harvest Hills Middle (HHM; 38°59’05.5” N, 95°27’19.0” W); and Cain (38°59’21.9” N, 95°25’19.9” W). All sites have similar landscape and management characteristics. Specifically, they: 1) are terraced with ridges and depressions across the landscape, 2) have perforated standpipes located in the depressions, that are connected to the tile outlet to help drain standing water, and 3) have tile drains that are all connected to wetlands

before being discharged to nearby streams, and eventually to Clinton Lake. HHN drains ~89,031 m^2 and consists of four terraces, HHM drains ~76,890 m^2 and consists of 3 terraces, whereas Cain drains ~161,874 m^2 and consists of six terraces. While Cain as the largest contributing area, tile density is lowest at 0.37 tiles/km^2 and increases to HHM at 0.39 tiles/km^2 and HHN at 0.44 tiles/km^2. We expect both drainage area and tile density will affect influent discharge and solute concentrations as might crop rotation given nitrogen fixing soybeans were rotated with wheat and corn crops on all three field over the duration study (Table 1).

Table 1. Crop type for the growing seasons for 2014 - 2018. The Cain site for 2016 - 2018 had mixed crops of alternating corn-soybean.

	Crop Type															
	HHM					HHN					Cain					
Year	2014	2015	2016	2017	2018	2014	2015	2016	2017	2018	2014	2015	2016	2017	2018	
Soybean	X		X	X	X	X		X	X	X	X	X	X	X	X	
Corn		X					X						X	X	X	
Winter Wheat	X	X				X	X									

The agricultural research sites are located approximately 29 km west of Lawrence, Kansas and roughly 2 miles separate the research sites. The general lithology of Douglas county (which encompasses the research sites), consists of limestone, shale, and sandstone (http://www.kgs.ku.edu/General/Geology/Douglas/geog01.html). The three study sites consist entirely of Argiudolls soil, a Great Group of the Mollisol order that are found in humid climates with an udic moisture regime. The average annual temperature is 12.4 ºC with reaching a high of 30.3 ºC in the summer and low of -6.3 ºC in the winter, while average annual precipitation is 960 mm with ~70% of the total precipitation falling in the spring and summer months (NOAA; 1981-2010 monthly normals: https://w2.weather.gov/climate/xmacis.php?wfo=top). Approximately 75% of the total precipitation falls within the growing season, which spans ~196 days (Kansas Geological Survey (KGS); www.kgs.ku.edu).

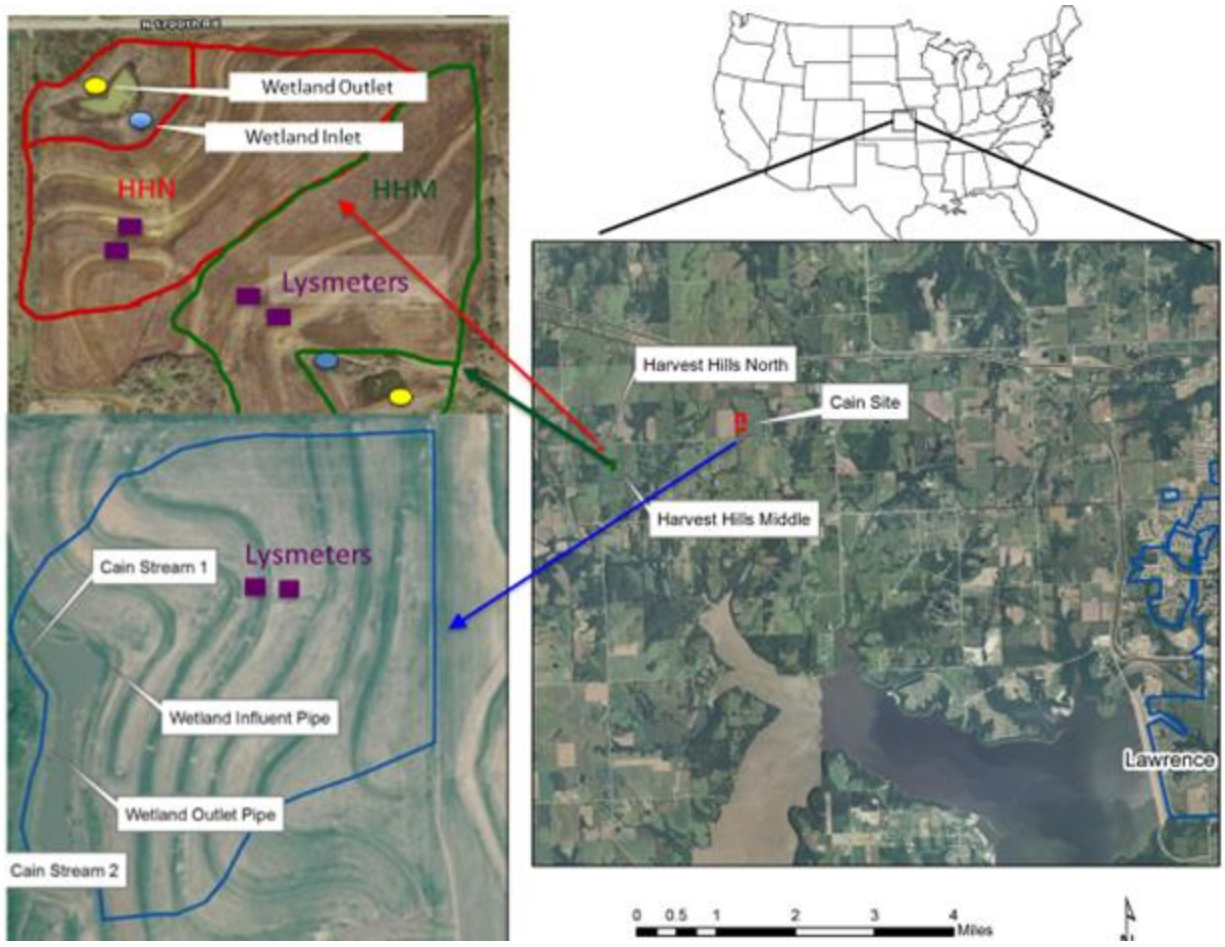

Figure 3. Harvest Hill North (HHN; outlined in red) and Middle (HHM; outlined in green) and Cain (outlined in blue) fields are located in Douglas County, Kansas. These sites drain into the Clinton Lake Reservoir. Blue circles on the left figure indicate approximate location of tile drains into the wetland while yellow circles indication outlet drains from wetlands to nearby streams. Purple boxes on left hand figure also indicate positions of soil suction cup lysimeters.

3 Methods

The sampling setup was comprised of automated samplers (ISCO Model 6712 Full-Size Portable) positioned at the inlet ("influent") and outlet ("effluent") of constructed retention ponds/wetlands on the three study sites (see Figure 3). Automated samplers were outfitted at the inlet and outlets of all three sites, where inlets measured velocity (m/s) using and ISCO (Model 750) and precipitation (mm) with a standard rain gauge tipping bucket (674 Tipping Rain, ISCO), and outlets measured water level (m) with a pressure transducer (Model 720, ISCO). Due to the design of the retention ponds, the outlets used two different configurations to measure

water fluxes from the wetlands toward the stream. The Model 750 area-velocity module is accurate to ± 0.03048 m/s for velocity and ± 0.00244 m/s for water levels, while the Model 720 ISCO pressure transducer is accurate to ± 0.003 m for a stage height range of 0.03 m to 1.52 m. All measurements were collected at 1-minute intervals continuously during the growing season of 2016-2018; generally starting in May/June through October. Due to instrument error with the rain-gauges, errors in the precipitation data were replaced with the nearest weather observatory (Clinton Lake; https://w2.weather.gov/climate/index.php?wfo=top) precipitation data.

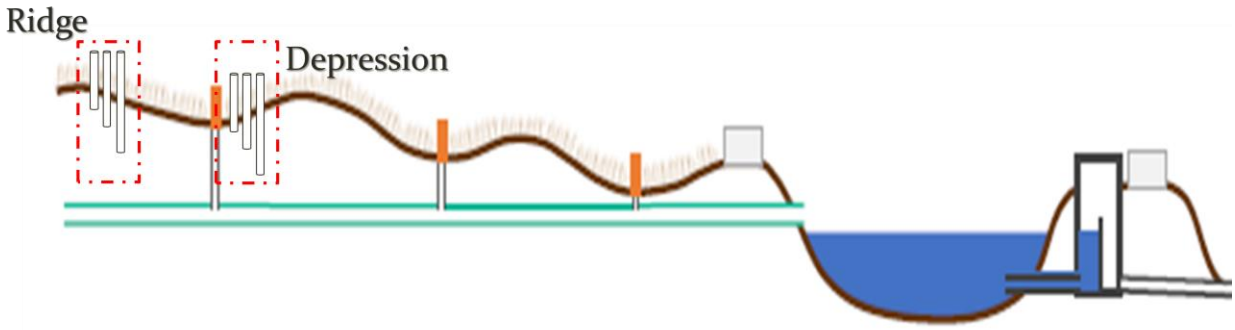

Figure 4. Conceptual diagram of tile outlet terrace (TOT) drainage system with receiving storage pond. Suction cup lysimeters were placed at 30, 60, and 90 cm, are outlined with red dashed lines are located at top (Ridge) of terrace and at bottom (Depression) of terrace.

3.1 Water sample collection

To characterize the response of TOTs and wetland discharge chemistry, and to use the chemical behavior to constrain recession curve analysis, storm event discharge samples were collected using programmed ISCO autosamplers at 15- or 30-min rates of collection depending on observed flow duration. Collection began once flow duration or stage surpass either 1.0 m/s or 0.1524 m and continued until the end of the flow event or until 24 bottles were collected (capacity of ISCO samplers). Bottles were collected from the field within 24-48 hrs of events, transported back to the University of Kansas Engineering Lab and sequentially filtered (see below). Weekly to bi-monthly wetland grab samples were also collected over the duration of the project and filtered in the same sequential methods as the event samples (see below). The wetland samples were collected due to high evaporation compared to precipitation rates in the summer, resulting in no effluent. The wetland samples allowed for better characterization of TOTs on wetland systems.

Sources of solute contributing to runoff at the TOTs were quantified using soil water suction cup lysimeters (SK20, Decagon; Figure 4) nested at depths of 30 cm, 60 cm, and 90 cm at two landscape positions: the ridge of a terrace and at the base of the terrace for each site (Figure 2, red dashed lines). Suction of 90 kPa was applied at least a week before each sampling event. These samples were filtered using a 0.45µm filter for anion and cations analysis.

3.2 Filtering and water chemical analyses

Event and grab samples were sub sampled and preserved according to proper standard laboratory methods, given enough sample (≥ 500 mL): 60 ml of unfiltered water was used for total nitrogen (TN) and phosphorus (TP) analysis; 250 ml was filtered through a 0.8µm filter for suspended solids analysis (see below), 60 ml of this filtrate was used for total dissolved nitrogen (TDN) and phosphorus (TDP), and 120 ml of the filtrate was passed through 0.45 µm filter for anion and cation analysis. Both hydrochloric (HCl) and nitric (HNO_3) acids were used for preservation, HCl for cation analysis by Ion Chromatography and HNO_3 for cation analysis by ICP-OES. A brief description of each method is provided in the following:

a. Nitrogen and Total Dissolved Nitrogen Analysis (TN and TDN): Water samples were analyzed for TN and TDN using the method of alkaline-persulfate oxidation of inorganic and organic nitrogenous compounds to nitrate according to Standard Methods 4500-NO3- (b) (APHA, 2005). Reactive nitrogen concentrations was determined colorimetrically using a Shimadzu 1650-PC UV/Visible light spectrophotometer at 220 nm and 275 nm.

b. Total Phosphorus and Total Dissolved Phosphorus Analysis (TP and TDP): Water samples were analyzed for TP and TDP using the method of acidic persulfate oxidation of organo-phosphate to inorganic orthophosphate according to Standard Method 4500-P (e) (APHA, 2005). Orthophosphate concentrations were determined colorimetrically using a Shimadzu 1650-PC UV/Visible light spectrophotometer at 885 nm.

c. Total Suspended Solids Analysis (TSS): TSS was measured for all water samples greater than 300 mL in volume. Pre-weighed 47 mm filter papers (Fisher Scientific #09-874-35 or equivalent) were dried for 24 hours in and oven at 100 to 105 ^{0}C then measured with a weighing tin prior to filtration of collected water. The filter paper was used in a vacuum filtration processes to remove

TSS from the water samples; the filter paper with residue was weighed and placed back in the oven at 100 to 105 ^{0}C for 24 hrs prior to final weighing.

d. Alkalinity and Anions: Alkalinity was measured on filtered (0.45 µm) water samples using the MetrOhm Titrando autotitrator. Anions were analyzed on filtered (0.45 µm) water samples using ion chromatography (Dionex ICS-1600). Anion activity was limited to three analytes: Chloride (Cl-), Nitrate (NO_3^-), and Sulfate (SO_4^{2-}).

e. Cations: Cations were analyzed on acidified (HCl), filtered (0.45 µm) water samples by ion chromatography (Dionex ICS-1600). Cation analysis was only limited by water sample availability; if there was low sufficient quantity, ion chromatography. If there was high availability, the ICP-OES was used.

3.3 Soil Collection and Analysis

Soil core samples were collected from each field site and tested for nutrient availability of nitrate-N and inorganic phosphate-P. Nitrate concentrations extracted from soil core samples were determined spectrophotometrically using the vanadium method of Doane & Horwath (2003). Inorganic phosphate concentrations extracted from soil core samples were determined spectrophotometrically using the malachite green method of D'Angelo et al. (2001).

3.4 Discharge Calculations

Water level and velocity (inlets only) measurements from the ISCOs at the inlets and outlets were used to determine discharge.

a. Inlets: Discharge (Q; m^3/s) at the inlets was determined as the product of the water velocity (m/s) and the water filled area (A; m^2) of the tile pipe. Here, A is solved using the following equation:

$$A = R^2/2 \cdot (\theta - \sin\theta)$$

where R is the radius (in m) of the circle and θ is the central angle in radians. In order to compare the functioning of TOTs between locations, we determine the specific discharge from the inlets by dividing Q by each respective field area.

b. Outlets: Given the two outlet configurations, different methods were applied at HHN and HHM compared to Cain for determining discharge. At HHN and HHM the outlet pipe

that drains the wetland goes to a weir box that is outfitted with a pressure transducer (Model 720, ISCO) and automated water sampler (ISCO Model 6712 Full-Size Portable Sampler). The outlet discharge (Q, m^3) from the HHN and HHM sites was calculated using a stage-discharge relationship:

$$Q = 3.33 \cdot L \cdot H \cdot 1.5$$

where L (m) is the length across the weir and H (m) is the height of water above the weir crest. At Cain, a culvert directly drains the wetland and water levels measured at the mouth of the culvert using a pressure transducer (Model 720, ISCO). Water samples were collected from inside the culvert using an automated water sampler (ISCO Model 6712 Full-Size Portable Sampler). For the Cain outlet, a culvert rating curve was employed:

$$Q = 1.511 \cdot S^2 - 3116.195 \cdot S + 1606117.046$$

where Q, discharge (ft^3) is related to S, stage (ft, elevation); the culvert rating curve can be found in the standard procedure for this monitoring project (Peltier et al., 2016). Discharge values where then converted from ft^3 to m^3.

3.5 Hydrograph Analysis

We used a recession curve analysis approach to determine the potential contributions of different water sources to the discharge signal derived from the influent. This method focuses on the part of the hydrograph from the peak of the rising limb to where the storm event response diminishes. The recession curve expresses the release of water from natural storages (Tallaksen, 1995). There are multiple conceptual methods used to quantify the recession curve. The general method derived from the work of Maillet (1905) is an exponential decay function expressed as:

$$Q_t = Q_o e^{-\alpha t}$$

Where Q_t is the discharge at time t, Q_o is the initial discharge, and α is the recession coefficient characterizing the aquifer. Barns (1939) replaced the exp(-α) with the constant, k, known as the recession constant or depletion factor. In this approach, the recession constant is graphed as log(Q) vs. time using the gradients of the three lines to infer the components of streamflow. The range of recession constants has been found to be approximately 0.2-0.8 for surface water (i.e.

conduit), 0.7-0.94 for interflow (i.e. intermediate), and 0.93-0.995 for base flow (i.e. diffuse), however there are issues with overlapping ranges (Nathan & McMahon, 1990).

To perform hydrograph separation analyses on the influent data, the respective discharges at each site was smoothed using a 15-minute sliding mean window that bracketed the actual measurement. Storm events where influent flow exceeded 0.05 m^3/s at Cain and HHN, 0.01 m^3/s at HHM, and had a duration greater than 10 minutes were used to understand the hydrologic response in TOT systems. We attempted three approaches to examine the potential flow paths contributing to the discharge signal. For successful approaches, we then examined their relationship to overall hydrologic state prior to the event, here defined as the precipitation received 1-day, 1-week, and 1-month prior to storm event flow,

3.5.1 EXPONENT FITTING APPROACH

The exponential decay function in eq. 1 is fit to the recession curve of a single storm event from the peak flow discharge of the hydrograph to where baseflow dominates. Barns (1939) suggested that individual components of hydrologic flow can be distinguished from the plotting of logarithm of flow versus time. The logged discharge can potentially be separated into characteristic components based on the response of flow with time.

3.5.2 RECURSIVE DIGITAL FILTER

This method approaches the discharge data as a "signal" in which a recursive digital filter is passed over the data and separates the signal based on high and low frequencies to distinguish quickflow (high frequency) and baseflow (low frequency). The filter is in the form:

$$f_k = af_{k-1} + (1 - a)/2\ (y_k - y_{k-1})$$

where f_k is the filtered quick response at the *k*th sampling instant (or the discharge at some given time after the onset of the event), y_k is the original streamflow, and *a* is the filter parameter; the filtered base flow is thus defined as $y_k - f_k$ (Nathan and McMahon, 1990). We used the digital recursive filter BaseflowSeparation function in the EcoHydRology R package (Fuka *et al.*, 2018). Here, we are able the digital filter parameter of 0.925 (recommended by Nathan and McMahon,1990) filters the total discharge analysis into two components baseflow and quickflow.

3.5.3 MASTER RECESSION CURVE APPROACH

A master recession curve (MRC) is an envelope of individual recession curves of short-term events (Figure 5). This method provides an average characterization of the most frequent depletion within the catchment and is represented by the recession constant, *k*. Various methods can be used to develop an MRC (Tallaksen, 1995), in the case of this study each exponential segment is interpreted to represent the depletion of the reservoir with the largest *k* indicating rapid movement, followed by an intermediate flow, and then by base or diffuse flow.

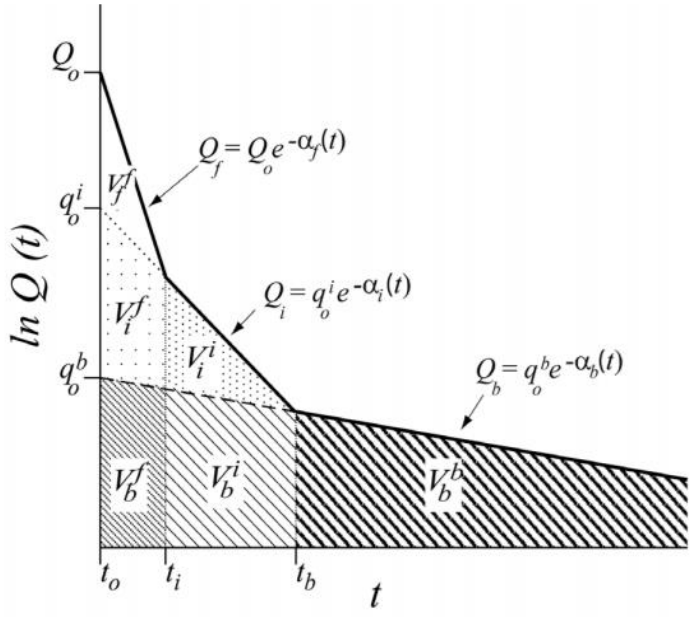

Figure 5. Representational schematic of a Master Recession Curve (MRC) with theoretical drainage volumes found by integration of each respective segment (Need to Cite this)

3.6 Mixing Model Analysis

Mixing models of streamflow assume that conservative tracers can be used to calculate the proportions of compositional end members that are mixed in sample waters. These proportions of end members can give an indication of geochemical processes. Seven potential end members will be examined for this approach: wet deposition (from National Atmospheric Deposition Program, NADP; *nadp.sws.uiuc.edu*) and soil water from ridge and base of the terraces at 30, 60 and 90 cm (see section 3.1 water sample collection). Here we used a simple

approach based on ratios for nitrate to chloride and sulfate to chloride to constrain source waters that feed stream flow during storm events.

3.7 Concentration Discharge (C-Q) Behavior and Weathering Fluxes

Two methods were used to determine if and how C-Q behavior from the fields differs with tile density and crop cover: 1) the slope (m) of the power law relationship ($C=aQ^m$) between solute concentrations and discharge (Godesy et al., 2009), and 2) solute concentration coefficient of variation (CV_c) and the discharge coefficient of variation (CV_q) (Thompson et al., 2011; Musolff et al., 2015). For the first method the C-Q is considered chemostatic or lacking a relationship between solute concentration and discharge when $m = 0$, conversely the relationship is considered chemodynamic or that solute concentrations are sensitive to changes in discharge when $m \neq 0$.

For the second method, chemostatic behavior is identified if the C-Q relationship exhibits low concentration variability ($CV_c/CV_q << 1$), while chemodynamic behavior is identified by large concentration variability ($CV_c/CV_q >> 1$). Once the contribution of water sources (e.g., conduit, intermediate and diffuse) has been determined for each precipitation event, the solute concentrations together with results from the end member mixing analysis are used to relate source waters and the biogeochemical signatures.

To determine weathering fluxes, we will focus on magnesium and silica concentrations in the influent discharge as they are likely act as proxies of weathering in this clay rich environment. Before calculating solute loads per event all influent solutes were corrected for wet deposition inputs using the following equation

$$[Xsol]_{corrected} = [Xsol]_E - ([Xsol]_P/[Cl]_P) * [Cl]_E$$

Where the corrected concentration, $[Xsol]_{corrected}$, is the difference of the concentration of the weathering solute of interest observed at the influent and product of the ratio of the weathering solute of interest in precipitation, $[Xsol]_p$, to that of the chloride in precipitation, $[Cl]_P$, and chloride concentration measured in the event, $[Cl]_E$. Here, we us chloride for correction as its greatest source is likely generated from atmospheric deposition. To determine the overall weathering flux, the corrected concentrations were then multiplied by the discharge to

determine the overall load which was then normalized to the area of each respective TOT for comparisons across systems.

4 Results

4.1 Precipitation and Discharge

Rainfall during the growing season over this three-year study were greatest in 2017 (796 mm) and lowest in 2018 (534 mm), which bookends the mean (685 mm). Generally speaking, the monthly distribution of rainfall was greatest early in the growing season compared to late in the growing season, except in 2018 (see figure 6).

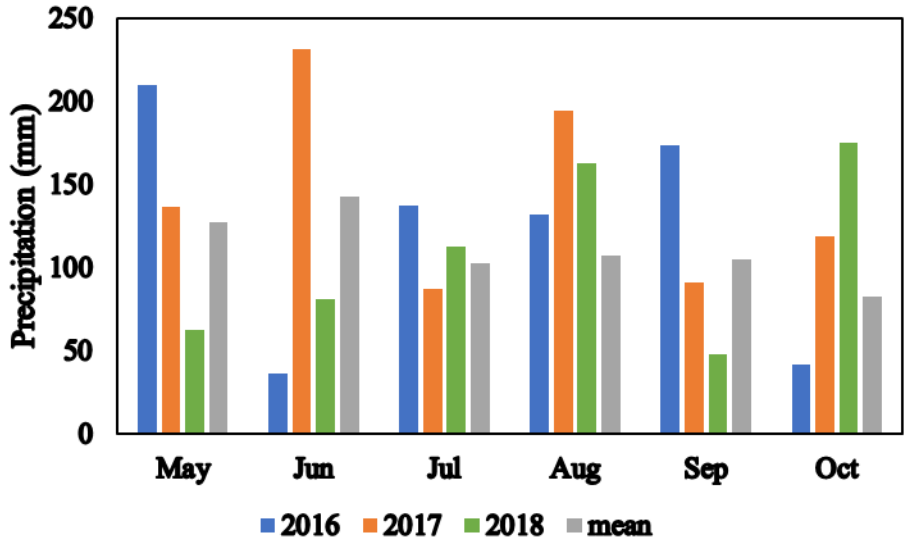

Figure 6. Total (colors: 2016 in blue, 2017 in orange, 2018 in green) monthly precipitation (mm) and monthly mean (grey; usclimatedata.com) at all sites between 2016-2018.

The median event based influent discharge for HHM, HHN, and Cain was ~25 m^3, ~442 m^3, and ~33 m^3 respectively, while median event effluent discharge was ~8335 m^3, ~5201 m^3, and ~0.40 m^3, respectively. The largest discharge events tended to occur early (May and June) and late (September and October) in the growing season, while much smaller events occurred at the height of the growing season (appendix 1, tables 3-5). This can be attributed to low rates of evapotranspiration compared to inputs of precipitation during early and late times in the growing

season. Figure 7 demonstrates that discharge behavior from the influent (orange) highly corresponds to precipitation events (dark blue; Figure 7a), while effluent discharge (light blue) often only corresponded to precipitation and influent behavior early in the growing season.

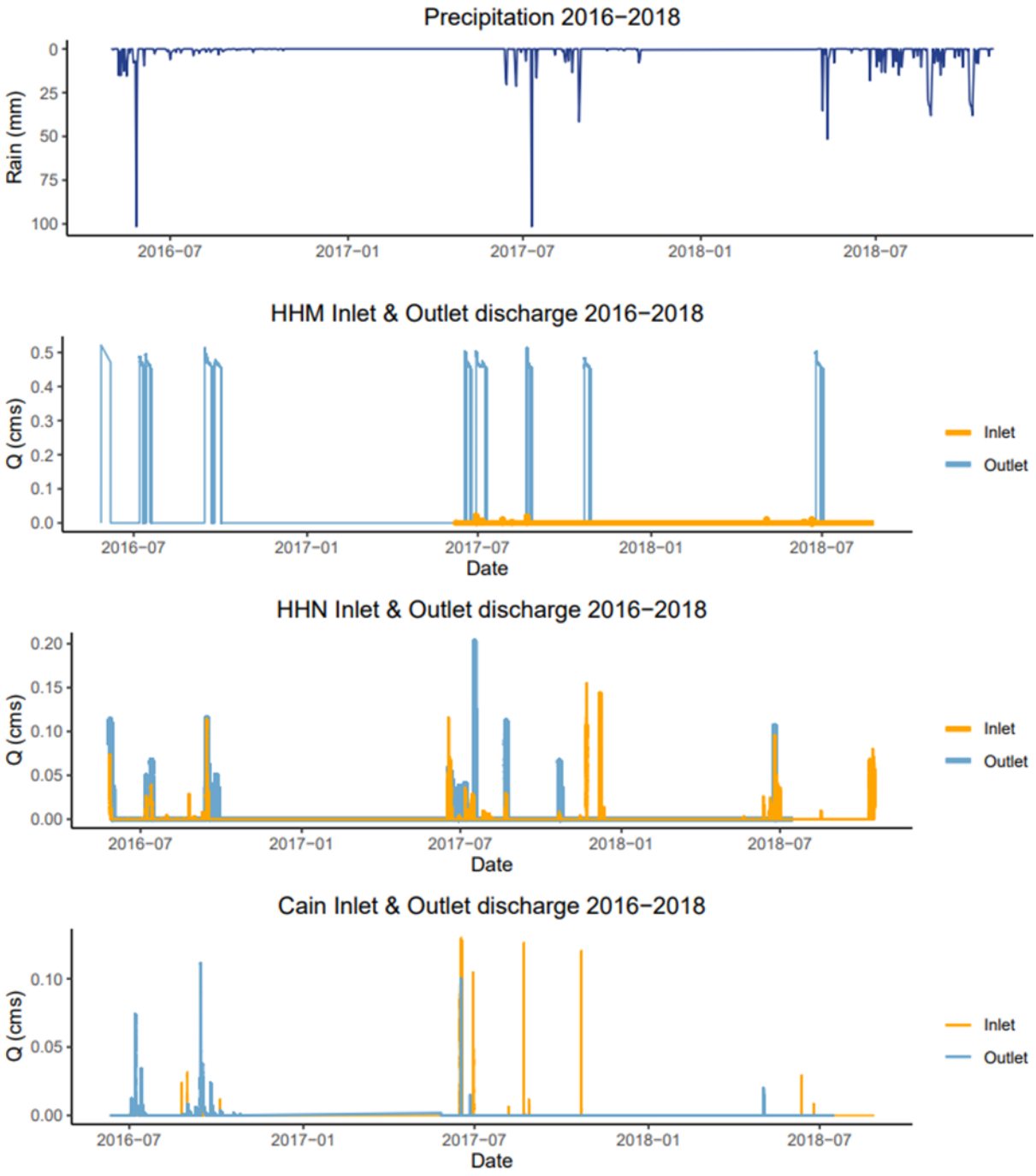

Figure 7. Precipitation (a), influent and effluent discharge (cms = m^3/s) at (b) HHM, (c) HHM, and (d) Cain.

Hydrograph responses at the inlets differed in terms of duration, frequency of events, and

rising-falling limb dynamics (Figure 8). Flow events at Cain were much longer in duration and size compared to HHN, while the smallest flow events and duration of events was observed at HHM. In addition, the response of the discharge curve following rain events differed for all sites with a much longer recession curve observed at the Cain site compared to HHN and HHM.

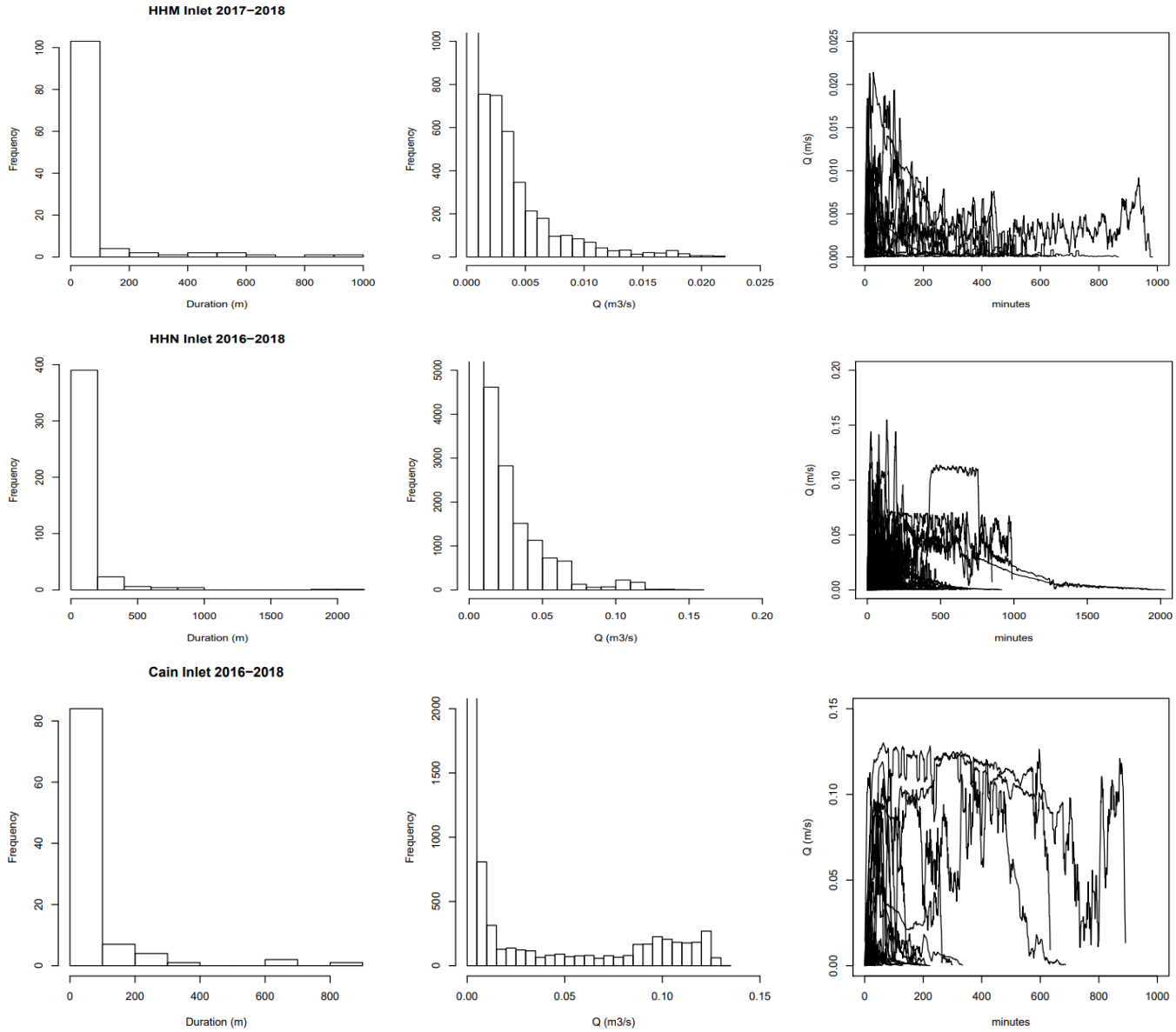

Figure 8. Flow patterns at HHM (top), HHN (middle) and Cain (bottom) for the 2016-2018 monitoring period. Flow duration (left), distribution of discharge (Q) events (center), and shape of Q events (right) amongst the sites.

4.2 Baseflow separation

We attempted to partition water ("quickflow" vs "baseflow") for each storm event using exponential fitting approaches (Barns, 1939) and then analyze each event to develop a master recession curve (review in Tallaksen, 1995). This technique, however, is not valid in these watersheds because it requires that discharge behave linearly in log space and tile influent discharge does not (Appendix 2). Specifically, for these techniques to work the intercepts of the log-linear lines that discern quick, intermediate, and base/diffuse flow must all decrease in order; at HHN, HHM and Cain the base/diffuse flow often had intercepts that exceeded those of quick and intermediate flow. Instead, baseflow separation was conducted using a recursive digital filter (Nathan and McMahon 1990) (Figure 9; appendix 2). All storm events where the resultant discharge was within one order of magnitude of the observed event discharge peak was used as a threshold to reduce the number of "small-fast" events, which, were often less than 10 minutes in duration, and/or instrument error. Quickflow dominated discharge composition early in events (Figure 9; quickflow represented as a difference between baseflow (red-dotted line) and total discharge (black line) and comprised most of the discharge if events were short in duration (~1 hr).

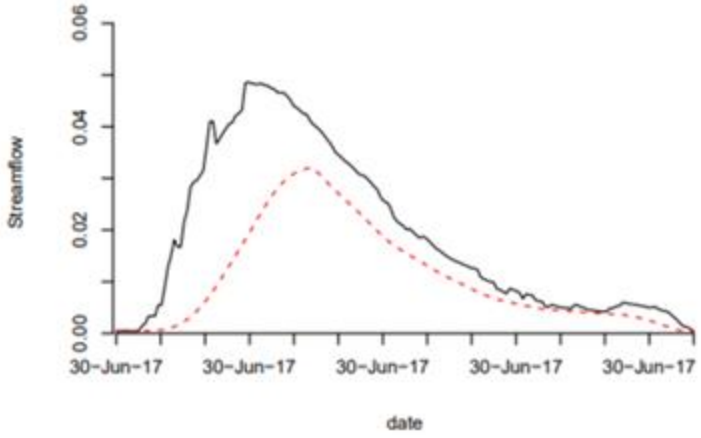

Figure 9. Example of baseflow separation using a digital recursive filter on influent discharge from Cain. Black line indicates total discharge and the red-dotted line indicates baseflow, the difference between the two represents

The proportion of baseflow from the total discharge was 38 %, 51%, and 46% for HHM, HHN, and Cain, respectively. The median baseflow for the three sites were 0.22 m^3/s, 3.5 m^3/s, and 0.24 m^3/s respectively. This metric indicates the degree of flashiness is greatest in HHM and lowest in HHN, yet the greatest discharge were observed at HHN. When we examined the relationship between precipitation a week prior to the event, we observed the strongest positive relationships when compared to the day and month prior to events (Figure 9). Cain and HHM

showed a greater response of proportion of flow to the 1-day and 1-month summed precipitation. Whereas, HHN showed a greater response of proportion of flow to the 1-week sum precipitation.

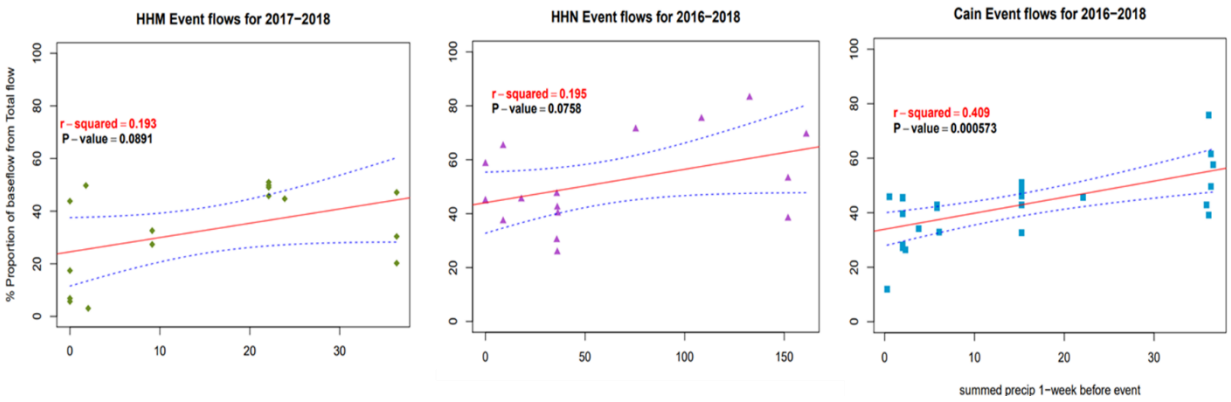

Figure 10. TOTs response to antecedent precipitation one week before flow events were captured. The blue dotted lines are the constrained standard error for the linear regression models of the three agriculture sites.

Interestingly, when we examined long duration storm events, which was observed to have the largest baseflow component as determined using the digital recursive filter (appendix 8, Tables 2-5), they had a very similar behavior across the sites, where discharge for the influent pipe remained high with a pulsed signature where discharge increased and decreased throughout the duration of the storm event. In comparison, short duration storm events maintained a much more typical “bell-shaped” hydrograph.

4.3 Water chemistry

4.3.1 INFLUENT AND EFFLUENT

The total (2016-2018) average concentrations for inlet data is shown in Figure 11. Of the nutrients measured, concentrations of nitrate (NO_3) were the highest followed by total nitrogen (TN), and then total dissolved nitrogen (TDN). Total phosphorus and total dissolved phosphorus make up a small proportion. Of the other ions concentrations of calcium were the highest, followed by sulfate (SO_4), sodium (Na), silica (Si) and chloride (Cl), and the remaining ions keep concentrations that were on average lower than 2.6 (mg/L).

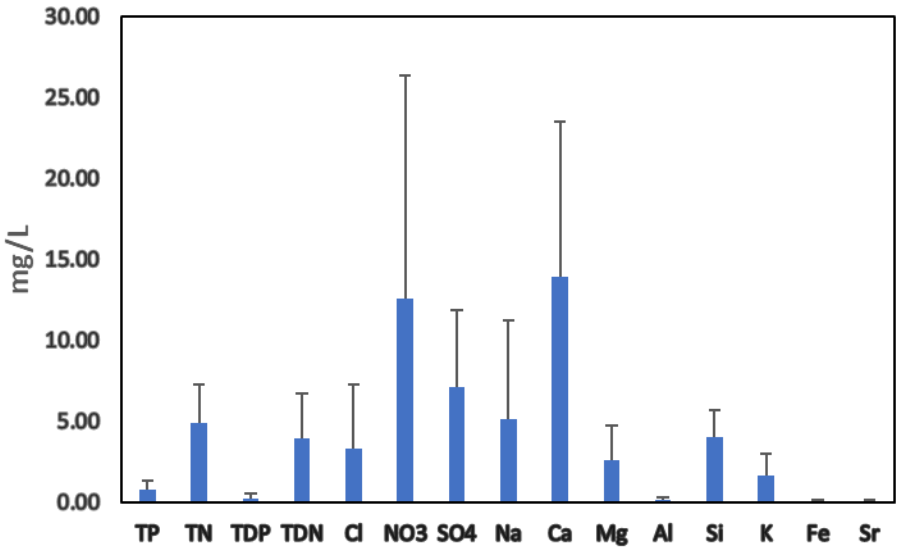

Figure 11. Average concentration and standard deviation of the influent water chemistry: total phosphorus (TP) total nitrogen (TN), total dissolved phosphorus (TDP), total dissolved nitrogen (TDN), chloride (Cl), nitrate (NO_3), sulfate (SO_4), sodium (Na), calcium (Ca), magnesium (Mg), aluminum (Al), silica (Si), potassium (K), manganese (Mn), iron (Fe), and strontium (Sr).

When we examine these concentrations for each of the influents between 2016-2018, we generally observe that most nutrients and solutes have the highest concentrations at the HHN sites (Figure 12). It must be noted that in the growing season of 2017 at the HHN site there was a

large amount of standing water that was not adequately drained which led to this increase of nutrient and solute concentrations.

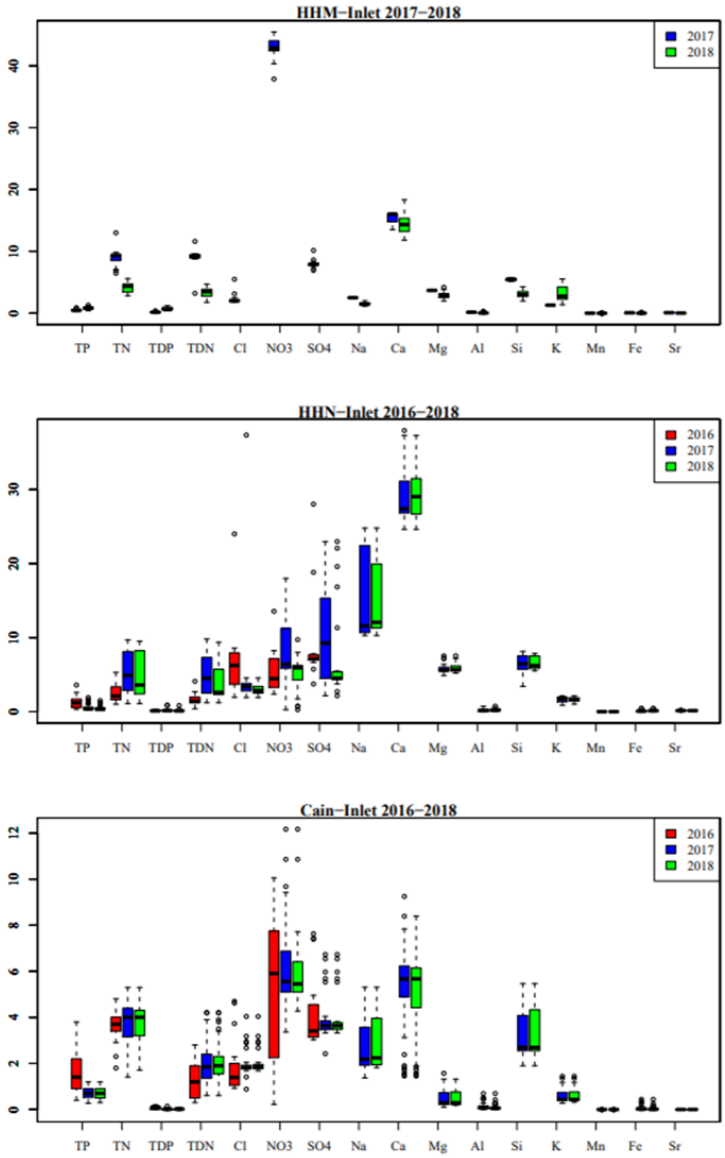

Figure 12. Average concentration and standard deviation of the influent water chemistry at HHM (top), HHN (middle), and Cain (bottom) from 2016-2018, samples were not collected form HHM in 2016. Chemistry includes: total phosphorus (TP), total nitrogen (TN), total dissolved phosphorus (TDP), total dissolved nitrogen (TDN), chloride (Cl), nitrate (NO_3), sulfate (SO_4), sodium (Na), calcium (Ca), magnesium (Mg), aluminum (Al), silica (Si), potassium (K), manganese (Mn), iron (Fe), and strontium (Sr).

4.3.2 LYSIMETERS

The largest concentrations were observed in HHN, where sulfate (SO_4) had the largest concentration at the "depression" (HHN.B) at ~6 mg/L, followed by nitrate (NO_3) at the "ridge" (HHN.T) at ~4 mg/L. Overall, HHN had a larger range of nutrient concentrations amongst the agriculture sites.

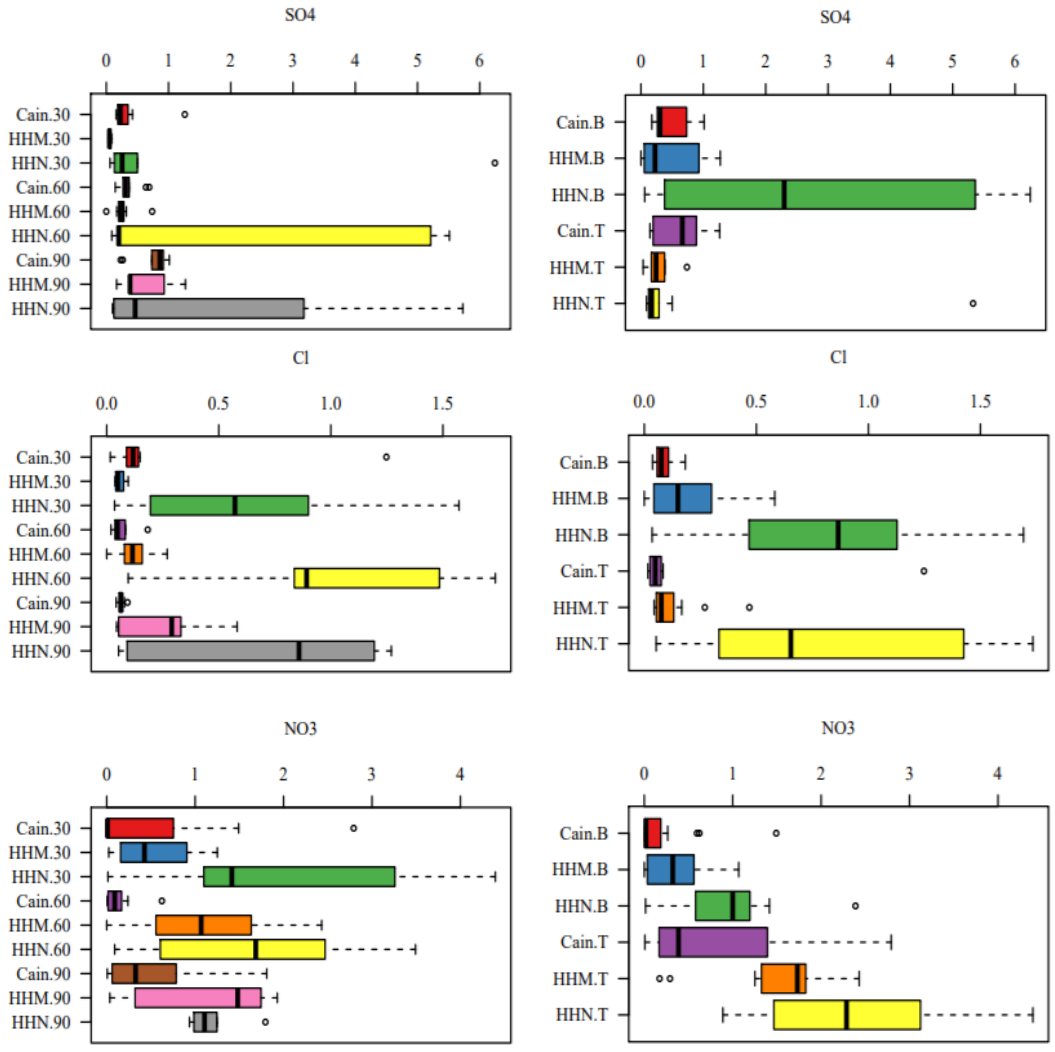

Figure 13. Average concentration and standard deviation of sulfate (SO_4; top), chloride (Cl; middle), and nitrate (NO3; bottom). All three sites at depth of 30, 60, and 90 cm are presented on the left, and on the right is presented the position of the lysimeters as "ridge" or tops (site. T) and "depressions" or bottoms (site. B).

4.4 Hydrograph Separation via End-member Mixing Models

To determine the source of water during storm events (quickflow vs. deeper flow) we compared the nitrate:chloride ratio to the sulfate:chloride ratio based on the assumption that nitrate is strongly influenced by agriculture and atmospheric inputs and sulfate is controlled predominately by geogenic inputs. Three distinct groupings were observed for each of the sites (Figure 14) where HHM (the smallest site) was closest to the atmospheric signature while Cain and HHN had signatures closer to the nested lysimeters. Interestingly, the difference between Cain and HHN is in their tendencies towards the precipitation signal, whereas Cain fell between the lysimeters and precipitation.

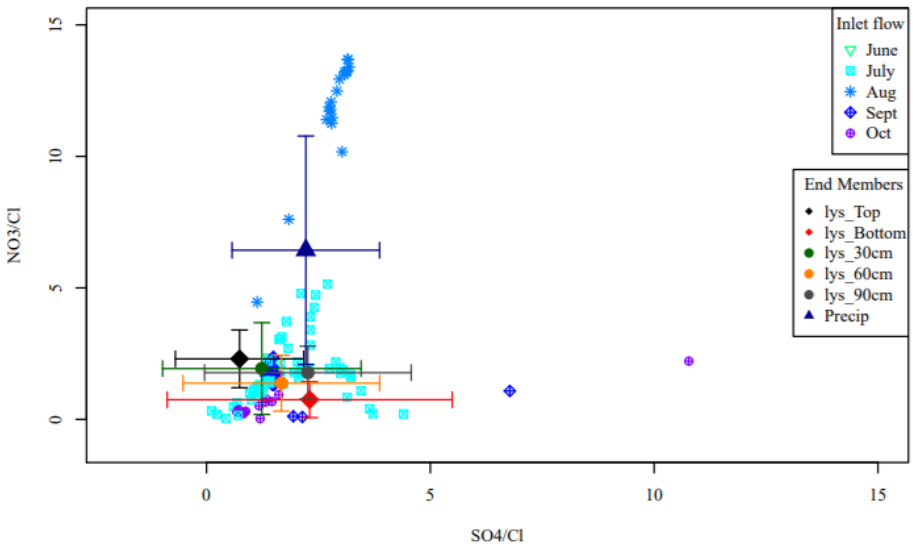

Figure 14. Mixing model for the agricultural inlet stream flow (June = light blue-green triangle, July = blue-green square, August = light blue asterisk, September = blue diamond cross, and October = purple circle cross) where the mean and standard deviation of known end members include lysimeters from ridge (lys_Top = black diamond) and the depression (lys_Bottom = red diamond) with the given depths of the lysimeters at 30 cm (lys_30cm = green circle), at 60 cm (lys_60cm = yellow circle), at 90 cm (lys_90cm = grey circle), and precipitation (blue triangle).

4.5 Concentration discharge behavior

To understand the connectivity of the tile-terraced fields to their discharge, we explored the concentration-discharge behavior over several storm events. Figure 15 shows the variability in concentrations over three of these events. Where total suspended solid (TSS) has elevated, total phosphorus (TP) concentrations were also elevated, but generally speaking total nitrogen

(TN) and dissolved nitrogen (TDN) were substantially higher than phosphorus and peaked around the peak discharge. We also observed that behavior of chloride (Cl) and sulfate (SO_4) differed among sites; with more variance observed in HHN compared to Cain.

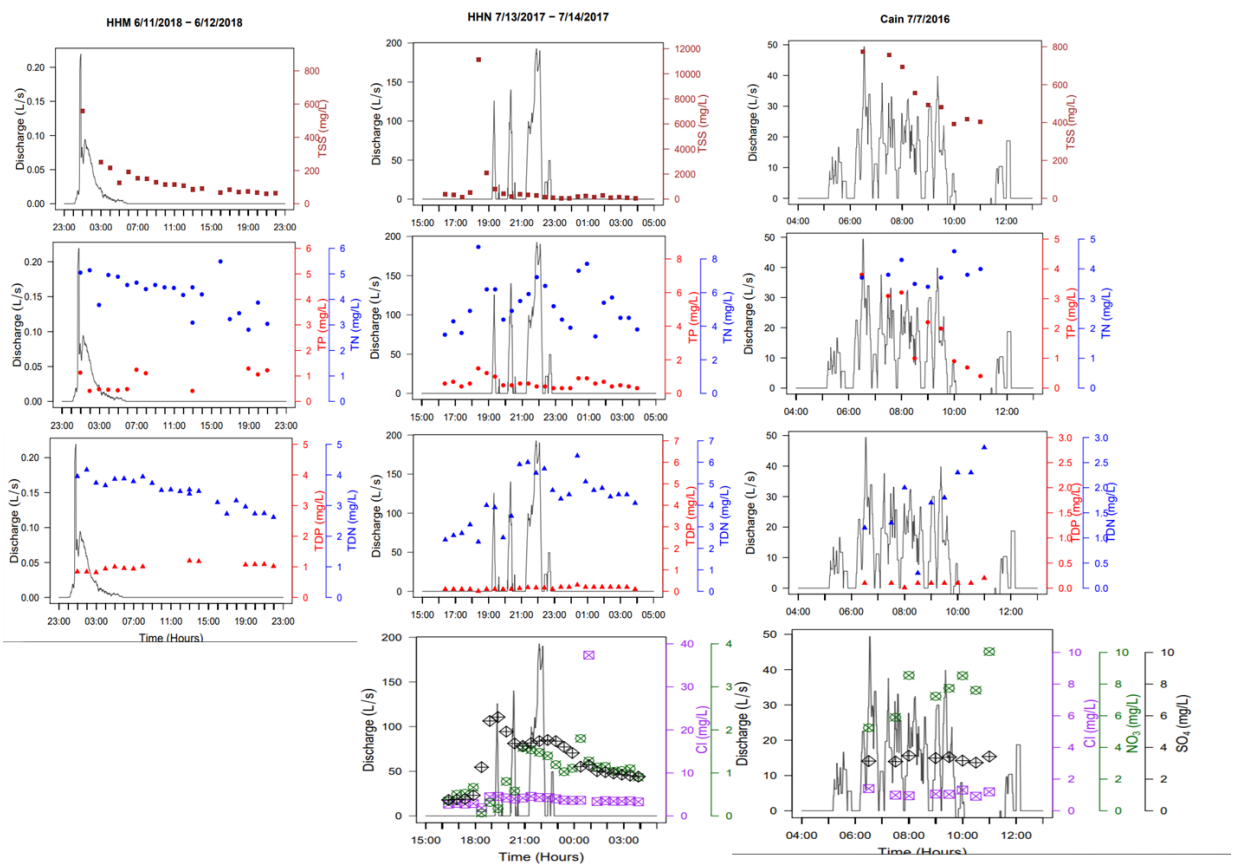

Figure 15. Discharge and water chemistry for event-based sampling for the HHM inlet on 6/11/2018, HHN inlet on 7/13/2017, and Cain inlet 7/7/2016; TSS (top, squares), TP and TN (top middle, circles), TDP and TDN (bottom middle, triangles), and Cl, NO_3, SO_4 (purple square cross, green circle plus, black diamond plus).

To gain a better picture of the behavior from all events, we examined the power law behavior of the C-Q relationships at each site for 16 solutes (Figure 5 see Appendix 8.3). Generally, the behavior of each solute across sites, rarely showed the same behavior, with the exception of TSS and TN which always show addition behavior and K that always shows dilution behavior. HHN and HHM had the greatest number of solutes that demonstrated addition behavior ($m > 0.02$), while most solutes at Cain demonstrated dilution behavior ($m < 0.01$), and only a couple solutes at any the sites showed chemostatic behavior. For example, HHN had five

solutes, the greatest number observed with chemostatic behavior (e.g., Na, Ca, Si, Sr, Mg). The CVc/CVq analysis showed most of the nutrients and solutes were chemostatic except for at HHN and Cain (see Figure 16). Nitrate and sulfate show an enrichment behavior at HHN, while total dissolved phosphorus (TDP) and strontium show chemodynamic behavior at Cain. When we pair these observations with observations of tile density and flashiness, we see that HHN and Cain show the greatest degree of chemodynamic behavior (evidenced from spreading in Figure 16), which in part agrees with our hypotheses, given that Cain is flashy and has a lower tile density. Interestingly, the data from HHN is inconsistent with our hypotheses, as we expected a more chemodynamic behavior to accompany higher tile densities and the less flashy hydrograph responses. One reason for this difference may be attributed to a more significant occurrence of surface erosion observed at HHN, as a result of poor/ineffective tile design.

Figure 16. Slope (b) of the stream water concentration-discharge (C-Q) compared to the coefficient of variation of the concentration to the discharge (CVc/CVq) for solutes at the three agriculture sites (HHM, HHN, and Cain) for the years 2016-2018

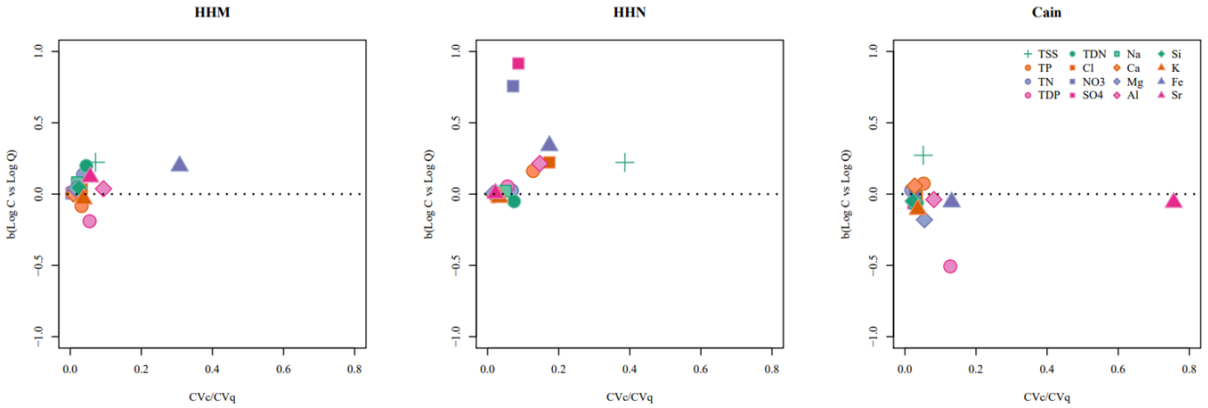

To better understand the impaction of tile-density, drainage area, and overall induced flashiness on these systems and on weathering fluxes, we focused on Mg and Si as they are likely the least impacted by artificial inputs associated with fertilizers. Here we calculated the total load of these to solutes discharged from the influent and removed the inputs associated with wet deposition. Estimated loads indicate that HHM and HHN had a larger load export than that of Cain in 2017. While the precipitation was similar amongst the three sites the contributing drainage area was similar for HHM and HHN with Cain being the largest. In relation to flashiness of these systems, the large export observed at HHN is in agreement with the slope of the power law for C-Q. This suggests that where our systems are less hydrologically flashy, they have a greater degree of chemodynamic behavior that generates the greatest proportion of weathered solutes.

Table 2. Solute (Mg/m^2) loads normalized by area for the three agriculture sites for 2017. Mg is corrected for wet deposition inputs. Negative solute loads indicate more solutes were retained in the catchment than was lost to influent discharge as a result of precipitation inputs.

Normalized Solute loads						
	HHM		HHN		Cain	
	Mg	Si	Mg	Si	Mg	Si
May	0	0	0	0	0	0
June	9.97	25.24	170.18	619.18	-20.60	210.90
July	6.69	11.80	89.78	125.22	0.00	0.00
Aug.	6.92	17.54	17.34	30.05	-8.76	96.03
Sept.	0.00	0.00	0.00	0.00	0.00	0.00
Oct.	0.00	0.00	4.13	5.58	-5.53	29.37

5 Discussion

Anthropogenic changes to the landscape have shifted the hydrologic response of landscapes and reduced residence time of water in agricultural environments (Kumar et al., 2018). It is well established in the literature that artificial manipulation to the land surface (e.g., tilling, berms, terraces) and subsurface drainage systems (e.g., tiles) increases inputs of event water and nutrient losses (Kladivko et al., 1999) from these systems. For example, tiled systems

have been found to behave more linearly than less-tiled drained watersheds, implying more homogenous flow paths in tile-drained systems (Shillings and Helmers, 2008). Here, we explored the less well-known impact of multiple, interacting surface and subsurface manipulations on landscape hydrology and the cascading biogeochemical response. Specifically, we focused on the interaction of tile and terrace manipulations as their hydrologic impacts differ—tiles move the energy from overland flow into the subsurface, thus reducing erosion (Kladivko et al., 2004; Goolsby et al., 1999), while terraces slow the energy of overland flow by reducing the topographic gradient (Shilling and Helmers, 2008; Kladivko et.al., 2004). Below we discuss the hydrologic and biogeochemical behavior observed between 2016-2018 on three agroecosystems under varying tile and terrace densities.

5.1 Hydrologic behavior across agroecosystems with varying tile-terrace densities

Our data illuminates the interactions of terraces and tiles leads to irregular storm water discharge events. When tiles are used alone, research has shown that typical exponential fitting and master recession curves can be used to understand the components of runoff that make up the discharge signal (Shillings and Helmers, 2008; Baedke and Krothe, 2001). When tile and terraces are paired together, we found that the characteristic flow response, when graphed, gave a different signal (appendix. 2) Given this response, the recursive digital filter was the best approach for separating components that contributed to discharge. Using the median baseflow discharge derived from the recursive digital filter as a metric for indicating "flashiness" or responsive to storm events (i.e., small values indicate greater "quickflow") for the TOT systems, we observed that HHM was the most responsive at 0.22 m^3/s, followed by Cain at 0.24 m^3/s, and then HHN at 3.5 m^3/s. These observations are consistent with the expected for hydrologic responsiveness to storm events or "flashiness" with varying tile-terrace densities as HHM and Cain had similar tile-terrace density of 0.39 and 0.37, respectively; while the HHN tile-terrace density was 0.44. These data are also consistent with literature that suggest more homogenous flow paths with increased tile-drained systems (Shillings and Helmers, 2008).

5.2 Spatial connectivity and depth control solute chemistry across TOT systems

In order to account for the range in the mixing model chemistry from seasonal variation throughout the sampling season, we assume that mixing from the end members would normally vary within one standard deviation from the mean. In general, the mixing model (Figure 14) end members (precipitation, lysimeters on top and bottom of the terraces) confine the influent waters across all sites. The lys_Top and lys_60cm end members are strong indicators for determining the source water during storm events (Figure 14). Using the data from Figure 13, the largest variation of NO_3 concentrations were found at depths of 30 and 60 cm on the ridges of the terraces. SO_4 were largest on the depression of terraces for all sites with the largest variations found at depths of 60 and 90 cm (Figure 13). This indicates that during storm events shallow ridges are a large source for NO_3. The spatial connectivity is greatest during June and July when antecedent moisture conditions are at their peak within the landscape. This depth control of solute chemistry and spatial connectivity in TOT systems is further strengthened by the generally larger load exports during the months of June and July (Table 2).

5.3 Greater tile-terrace densities support more chemodynamic behavior and greater weather fluxes

While greater tile-terrace densities decreased hydrologic flashiness they increased the degree of chemostatic behavior contrary to our hypothesis and all together supported a greater estimated weathering flux. This behavior was observed at the HHN site, where tile-terrace design had several issues that led to ponding and greater overland erosion; which could possibly have increased water residence time and resulted in a greater transformation and mobilization compared to HHM and Cain. Given that the same soil series and grainsize distributions underlie the soils in these three agroecosystems it is possible this behavior results from historical loading not accounted for when estimating inputs from wet deposition alone.

6 Conclusion

The study of storm events in agricultural fields is useful in identifying mechanisms of nutrient transport and transformation during runoff events under varying antecedent soil moisture

conditions and growing conditions. Anthropogenic altered landscapes (artificial subsurface drainage and terraces), and their resultant changed hydrology of the landscape affects the transformation, transport, and fate of applied fertilizers and their effect on other solute behavior. The interaction of terrace and tile outlets leads to irregular storm water discharge events when graphed, revealed that the characteristic hydrological flow response gave a different signal. The density of terraces to tile outlets corresponds with our hypothesis in terms of flashiness of discharge and solute loads. However, the CVc/CVq data from HHN is inconsistent with our hypotheses, as we expected a more chemostatic behavior to accompany higher tile densities and the less flashy hydrograph responses (see Figure 16). In general, higher tile densities led to lower hydrologic flashiness but greater chemodyanmic behavior, specifically addition behavior and greater weathering fluxes. This study showed that part of the hypotheses was supported but other factors need to be considered when thinking about the C-Q behavior and weathering fluxes.

7 References

Alexander, L. V., Zhang, X., Peterson, T. C., Caesar, J., Gleason, B., Tank, A. K., ... & Tagipour, A. (2006). Journal of Geophysical Research: Atmospheres, 111(D5).

Andrews, J. A., & Schlesinger, W. H. (2001). Soil CO2 dynamics, acidification, and chemical weathering in a temperate forest with experimental CO2 enrichment. Global Biogeochemical Cycles, 15(1), 149-162.

Baedke, S. J., & Krothe, N. C. (2001). Derivation of effective hydraulic parameters of a karst aquifer from discharge hydrograph analysis. Water resources research, 37(1), 13-19.

Barak, P., Jobe, B. O., Krueger, A. R., Peterson, L. A., & Laird, D. A. (1997). Effects of long-term soil acidification due to nitrogen fertilizer inputs in Wisconsin. Plant and soil, 197(1), 61-69.

Barnes, B. S. (1939). The structure of discharge-recession curves. Eos, Transactions American Geophysical Union, 20(4), 721-725.

Berner, R. A., Lasaga, A. C., & Garrels, R. M. (1983). The carbonate-silicate geochemical cycle and its effect on atmospheric carbon dioxide over the past 100 million years. American Journal of Science, 283, 641-683.

Blann, K. L., Anderson, J. L., Sands, G. R., & Vondracek, B. (2009). Effects of agricultural drainage on aquatic ecosystems: a review. Critical reviews in environmental science and technology, 39(11), 909-1001.

Bowes, M. J., Jarvie, H. P., Halliday, S. J., Skeffington, R. A., Wade, A. J., Loewenthal, M., ... & Palmer-Felgate, E. J. (2015). Characterizing phosphorus and nitrate inputs to a rural river using high-frequency concentration–flow relationships. Science of the Total Environment, 511, 608-620.

Brodie, R. S., & Hostetler, S. (2005, November). A review of techniques for analysing baseflow from stream hydrographs. In Proceedings of the NZHS-IAH-NZSSS 2005 conference (Vol. 28). Auckland New Zealand.

Bruinsma, J. (2017). World agriculture: towards 2015/2030: an FAO study. Routledge.

Burns, D. A., McDonnell, J. J., Hooper, R. P., Peters, N. E., Freer, J. E., Kendall, C., & Beven, K. (2001). Quantifying contributions to storm runoff through end-member mixing analysis and hydrologic measurements at the Panola Mountain Research Watershed (Georgia, USA). Hydrological processes, 15(10), 1903-1924.

Cosby, B. J., Hornberger, G. M., Galloway, J. N., & Wright, R. F. (1985). Modeling the effects of acid deposition: Assessment of a lumped parameter model of soil water and streamwater chemistry. Water Resources Research, 21(1), 51-63.

D'Angelo, E., Crutchfield, J., & Vandiviere, M. (2001). Rapid, sensitive, microscale determination of phosphate in water and soil. Journal of environmental quality, 30(6), 2206-2209.

Dewandel, B., Lachassagne, P., Bakalowicz, M., Weng, P. H., & Al-Malki, A. (2003). Evaluation of aquifer thickness by analysing recession hydrographs. Application to the Oman ophiolite hard-rock aquifer. Journal of hydrology, 274(1-4), 248-269.

Doane, T.A., & Horwath, W. R. (2003). Spectrophotometric determination of nitrate with a single reagent. Analytical letters, 36(12), 2713-2722.

Dreiss, S. J. (1989). Regional scale transport in a karst aquifer: 1. Component separation of spring flow hydrographs. Water Resources Research, 25(1), 117-125.

Drever, J. I. (1994). The effect of land plants on weathering rates of silicate minerals. Geochimica et Cosmochimica Acta, 58(10), 2325-2332.

Driscoll, C. T., Lawrence, G. B., Bulger, A. J., Butler, T. J., Cronan, C. S., Eagar, C., ... & Weathers, K. C. (2001). Acidic Deposition in the Northeastern United States: Sources and Inputs, Ecosystem Effects, and Management Strategies: The effects of acidic deposition in the northeastern United States include the acidification of soil and water, which stresses terrestrial and aquatic biota. AIBS Bulletin, 51(3), 180-198.

Federation, W. E. & Association, A. P. H. (2005). Standard methods for the examination of water and wastewater. American Public Health Association (APHA): Washington, DC, USA.

Foley, Jonathan A., et al. "Global consequences of land use." science 309.5734 (2005): 570-574.

Fuka DR, Walter MT, Archibald JA, Steenhuis TS and Easton ZM (2018). EcoHydRology: A Community Modeling Foundation for Eco-Hydrology. R package version 0.4.12.1. https://CRAN.R-project.org/package=EcoHydRology

Gedney, N., Cox, P. M., Betts, R. A., Boucher, O., Huntingford, C., & Stott, P. A. (2006). Detection of a direct carbon dioxide effect in continental river runoff records. Nature, 439(7078), 835.

Gleick, Peter H. "Water use." Annual review of environment and resources 28.1 (2003): 275-314.

Godsey, S. E., Kirchner, J. W., & Clow, D. W. (2009). Concentration–discharge relationships reflect chemostatic characteristics of US catchments. Hydrological Processes: An International Journal, 23(13), 1844-1864.

Goolsby, D. A., Battaglin, W. A., Lawrence, G. B., Artz, R. S., Aulenbach, B. T., Hooper, R. P., & Stensland, G. J. (1999). Flux and sources of nutrients in the Mississippi-Atchafalaya River Basin. National Oceanic and Atmospheric Administration National Ocean Service Coastal Ocean Program.

Gruber, N., & Galloway, J. N. (2008). An Earth-system perspective of the global nitrogen cycle. Nature, 451(7176), 293.

Guo, J., Wang, F., Vogt, R. D., Zhang, Y., & Liu, C. Q. (2015). Anthropogenically enhanced chemical weathering and carbon evasion in the Yangtze Basin. Scientific reports, 5, 11941.

Hall, F. R. (1968). Base-flow recessions—A review. Water Resources Research, 4(5), 973-983.

Harman, C. J., Rao, P. S. C., Basu, N. B., McGrath, G. S., Kumar, P., & Sivapalan, M. (2011). Climate, soil, and vegetation controls on the temporal variability of vadose zone transport. Water Resources Research, 47(10).

Herndon, E. M., Dere, A. L., Sullivan, P. L., Norris, D., Reynolds, B., & Brantley, S. L. (2015). Landscape heterogeneity drives contrasting concentration–discharge relationships in shale headwater catchments. Hydrology and Earth System Sciences, 19(8), 3333-3347.

Jeannin, P. Y., & Sauter, M. (1998). Analysis of karst hydrodynamic behaviour using global approaches: a review. Bull. Hydrogéol.(Neuchâtel), 16, 31-48.

Kladivko, E. J., Frankenberger, J. R., Jaynes, D. B., Meek, D. W., Jenkinson, B. J., & Fausey, N. R. (2004). Nitrate leaching to subsurface drains as affected by drain spacing and changes in crop production system. Journal of Environmental Quality, 33(5), 1803-1813.

Koenig, L. E., Shattuck, M. D., Snyder, L. E., Potter, J. D., & McDowell, W. H. (2017). Deconstructing the effects of flow on DOC, nitrate, and major ion interactions using a high-frequency aquatic sensor network. Water Resources Research, 53(12), 10655-10673.

Kovács, A., & Perrochet, P. (2008). A quantitative approach to spring hydrograph decomposition. Journal of hydrology, 352(1-2), 16-29.

Kumar, P., Le, P. V., Papanicolaou, A. T., Rhoads, B. L., Anders, A. M., Stumpf, A., ... & Filley, T. (2018). Critical transition in critical zone of intensively managed landscapes. Anthropocene, 22, 10-19.

Kump, L. R., Brantley, S. L., & Arthur, M. A. (2000). Chemical weathering, atmospheric CO2, and climate. Annual Review of Earth and Planetary Sciences, 28(1), 611-667.

Li, L., Bao, C., Sullivan, P. L., Brantley, S., Shi, Y., & Duffy, C. (2017). Understanding watershed hydrogeochemistry: 2. Synchronized hydrological and geochemical processes drive stream chemostatic behavior. Water Resources Research, 53(3), 2346-2367.

Maillet, E. T. (1905). Essais d'hydraulique souterraine & fluviale. A. Hermann.

McCorvie, M. R., & Lant, C. L. (1993). Drainage district formation and the loss of Midwestern wetlands, 1850-1930. Agricultural History, 67(4), 13-39.

Moatar, F., Abbott, B. W., Minaudo, C., Curie, F., & Pinay, G. (2017). Elemental properties, hydrology, and biology interact to shape concentration-discharge curves for carbon, nutrients, sediment, and major ions. Water Resources Research, 53(2), 1270-1287.

Musolff, A., Schmidt, C., Selle, B., & Fleckenstein, J. H. (2015). Catchment controls on solute export. Advances in water resources, 86, 133-146.

Nathan, R. J., & McMahon, T. A. (1990). Evaluation of automated techniques for base flow and recession analyses. Water resources research, 26(7), 1465-1473.

Palmer, A., Palmer, M., & Sasowsky, I. (Eds.). (1999). Karst modeling (Vol. 5). Karst Waters Institute.

Peltier, E.F., C.B.Y, Luellen, L., Lee, H. (2016). Monitoring effectiveness of tile outlet terrace fields with constructed wetlands for sediment, nutrient, and volume reduction in Northeastern Kansas. Report No. [Draft Version], (Topeka, KS, 2016).

Perrin, Anne-Sophie, Anne Probst, and Jean-Luc Probst. "Impact of nitrogenous fertilizers on carbonate dissolution in small agricultural catchments: implications for weathering CO2 uptake at regional and global scales." Geochimica et Cosmochimica Acta 72.13 (2008): 3105-3123.

Pielke, Roger A., et al. "The influence of land-use change and landscape dynamics on the climate system: relevance to climate-change policy beyond the radiative effect of greenhouse gases." Philosophical Transactions of the Royal Society of London A: Mathematical, Physical and Engineering Sciences 360.1797 (2002): 1705-1719.

Pinder, G. F., & Jones, J. F. (1969). Determination of the ground-water component of peak discharge from the chemistry of total runoff. Water Resources Research, 5(2), 438-445.

Raymond, P. A., Oh, N. H., Turner, R. E., & Broussard, W. (2008). Anthropogenically enhanced fluxes of water and carbon from the Mississippi River. Nature, 451(7177), 449.

Rehrl, C., & Birk, S. (2010). HYDROGEOLOGICAL CHARACTERISATION AND MODELLING OF SPRING CATCHMENTS IN A CHANGING ENVIRONMENT. Austrian Journal of Earth Sciences, 103(2).

Schilling, K. E., & Helmers, M. (2008). Tile drainage as karst: Conduit flow and diffuse flow in a tile-drained watershed. Journal of Hydrology, 349(3-4), 291-301.

Shuster, E. T., & White, W. B. (1971). Seasonal fluctuations in the chemistry of lime-stone springs: A possible means for characterizing carbonate aquifers. Journal of hydrology, 14(2), 93-128.

Steffen, W., Broadgate, W., Deutsch, L., Gaffney, O., & Ludwig, C. (2015). The trajectory of the Anthropocene: the great acceleration. The Anthropocene Review, 2(1), 81-98.

Sullivan, P. L., Stops, M. W., Macpherson, G. L., Li, L., Hirmas, D. R., & Dodds, W. K. (2018). How landscape heterogeneity governs stream water concentration-discharge behavior in carbonate terrains (Konza Prairie, USA). Chemical Geology.

Tallaksen, L. M. (1995). A review of baseflow recession analysis. Journal of hydrology, 165(1-4), 349-370.

Tang, C., Weligama, C., & Sale, P. (2013). Subsurface soil acidification in farming systems: Its possible causes and management options, Xu, J., & Sparks, D. L. (eds.). Molecular Environmental Soil Science. Springer Netherlands.

Thompson, S. E., Basu, N. B., Lascurain, J., Aubeneau, A., & Rao, P. S. C. (2011). Relative dominance of hydrologic versus biogeochemical factors on solute export across impact gradients. Water Resources Research, 47(10).

Waters, C. N., Zalasiewicz, J., Summerhayes, C., Barnosky, A. D., Poirier, C., Gałuszka, A., ... & Jeandel, C. (2016). The Anthropocene is functionally and stratigraphically distinct from the Holocene. Science, 351(6269), aad2622.

Wei, W., Chen, D., Wang, L., Daryanto, S., Chen, L., Yu, Y., ... & Feng, T. (2016). Global synthesis of the classifications, distributions, benefits and issues of terracing. Earth-science reviews, 159, 388-403.

White, W. B. (2002). Karst hydrology: recent developments and open questions. Engineering geology, 65(2-3), 85-105.

Zhang, Y., Zhang, Z., Ma, Z., Chen, J., Akbar, J., Zhang, S., ... & Cerdà, A. (2018). A review of preferential water flow in soil science. Canadian Journal of Soil Science, 98(4), 604-618.

8 Appendices

8.1 Appendix 1: Precipitation and discharge data

Table1. Monthly total precipitation (mm) and mean daily per month values and standard deviation for 2016-2018.

Month	2016	2017	2018	Mean
May	210.058	71.628	62.992	135.89
Jun	*17.272	231.648	81.026	149.098
Jul	137.668	87.63	33.528	104.902
Aug	132.08	194.31	133.35	103.124
Sep	173.736	91.44	48.006	106.934
Oct	41.656	119.38	175.26	85.09

Table 2. Discharge for the three sampling seasons 2016-2018.

	2016		2017		2018	
Site	Total Q	mean±sd	Total Q	mean±sd	Total Q	mean±sd
HHN	142.12	1.28 ± 7.00	106.4	0.86 ± 3.09	162.15	1.20 ± 5.31
HHM	--	--	11.13	0.075 ± 0.49	5.14	0.044 ± 0.22
Cain	8.29	0.06 ± 0.30	238.01	2.38 ± 11.70	0.7	0.006 ± 0.051

Table 3. HHM inlet storm events with baseflow, quickflow, and total discharge of storm events.

HHM Inlet Events

	Start	End	Time_diff	baseflow	quickflow	sum_Q	mean_Q	Tot_Q
1	6/29/2017 6:07	6/29/2017 6:39	32	0.06	0.24	0.30	0.0094	17.99
2	6/29/2017 6:42	6/29/2017 6:59	17	0.06	0.13	0.18	0.0107	10.87
3	6/29/2017 7:04	6/29/2017 9:51	167	0.59	0.66	1.25	0.0075	74.83
4	6/29/2017 10:07	6/29/2017 14:32	265	2.13	0.61	2.74	0.0104	164.66
5	6/30/2017 2:50	6/30/2017 4:25	95	0.15	0.19	0.34	0.0036	20.32
6	7/5/2017 14:55	7/5/2017 15:24	29	0.03	0.08	0.11	0.0037	6.46
7	7/5/2017 15:30	7/5/2017 16:04	34	0.04	0.07	0.11	0.0033	6.65
8	7/26/2017 0:00	7/27/2017 0:00	1440	0.22	1.06	1.28	0.0009	77.09
9	7/27/2017 11:20	7/27/2017 11:53	33	0.00	0.06	0.07	0.0021	4.17
10	7/27/2017 11:56	7/27/2017 12:13	17	0.00	0.04	0.04	0.0024	2.49
11	7/27/2017 12:16	7/27/2017 19:32	436	0.50	0.64	1.13	0.0026	68.07
12	8/21/2017 0:00	8/22/2017 0:00	1440	0.24	0.23	0.47	0.0003	27.96
13	8/22/2017 0:03	8/22/2017 2:09	126	0.63	0.63	1.26	0.0100	75.54
14	8/22/2017 2:13	8/22/2017 2:29	16	0.04	0.05	0.09	0.0058	5.52
15	8/22/2017 4:41	8/22/2017 9:20	279	0.38	0.39	0.77	0.0027	45.94
16	5/3/2018 12:58	5/3/2018 20:44	466	1.46	0.86	2.32	0.0050	139.05
17	6/12/2018 0:05	6/12/2018 5:47	342	0.29	0.13	0.42	0.0012	25.27
18	6/19/2018 12:35	6/19/2018 13:07	32	0.00	0.09	0.09	0.0027	5.27
19	6/20/2018 7:04	6/20/2018 23:27	983	0.88	0.89	1.76	0.0018	105.73

Table 4. HHN inlet storm events with baseflow, quickflow, and total discharge of storm events.

HHN Inlet Events

	Start	End	Time_diff	baseflow	quickflow	sum_Q	mean_Q	Tot_Q
1	5/27/2016 0:00	5/28/2016 0:00	1440	43.22	8.78	52.01	0.0361	3120.35
2	9/13/2016 0:00	9/15/2016 0:00	2880	49.61	7.10	56.71	0.0197	3402.55
3	6/17/2017 0:46	6/17/2017 2:25	99	1.29	1.43	2.72	0.0275	163.17
4	6/17/2017 16:45	6/17/2017 17:21	36	0.51	1.17	1.67	0.0465	100.47
5	6/17/2017 18:18	6/17/2017 19:57	99	0.33	1.75	2.07	0.0209	124.27
6	6/18/2017 20:44	6/18/2017 23:49	185	2.03	2.76	4.79	0.0259	287.55
7	6/19/2017 10:00	6/19/2017 17:17	437	2.03	5.83	7.86	0.0180	471.68
8	6/19/2017 0:00	6/20/2017 0:00	1440	4.71	7.03	11.74	0.0082	704.53
9	11/22/2017 1:44	11/22/2017 4:41	177	4.04	6.80	10.84	0.0613	650.52
10	11/22/2017 6:42	11/22/2017 9:28	166	7.36	3.93	11.29	0.0680	677.34
11	12/6/2017 0:00	12/7/2017 0:00	1440	6.56	4.65	11.21	0.0078	672.37
12	12/8/2017 8:02	12/8/2017 11:52	230	3.07	3.80	6.87	0.0299	412.21
13	6/24/2018 19:15	6/24/2018 23:51	276	4.07	5.01	9.08	0.0329	544.55
14	6/25/2018 12:31	6/25/2018 15:30	179	2.54	2.37	4.91	0.0274	294.69
15	6/26/2018 10:22	6/26/2018 12:19	117	1.46	1.76	3.22	0.0275	193.39
16	10/11/2018 7:33	10/11/2018 8:26	53	1.01	1.63	2.65	0.0500	158.94
17	10/11/2018 8:35	10/11/2018 10:00	85	2.18	1.92	4.10	0.0483	246.24
18	10/13/2018 3:01	10/13/2018 5:04	123	4.00	1.76	5.76	0.0468	345.57
19	10/14/2018 0:00	10/15/2018 0:00	1440	34.80	11.43	46.23	0.0321	2773.94
20	10/15/2018 0:00	10/16/2018 0:00	1440	21.95	8.81	30.76	0.0214	1845.52

Table 5. Cain inlet storm events with baseflow, quickflow, and total discharge of storm events.

Cain Inlet Events

	Start	End	Time_diff	baseflow	quickflow	sum_Q	mean_Q	Tot_Q
1	7/7/2016 6:11	7/7/2016 6:51	40	0.14	0.30	0.44	0.0110	26.30
2	7/7/2016 7:06	7/7/2016 7:47	41	0.18	0.21	0.39	0.0095	23.39
3	7/7/2016 7:52	7/7/2016 8:43	51	0.23	0.22	0.46	0.0089	27.30
4	7/7/2016 8:54	7/7/2016 9:11	17	0.07	0.09	0.16	0.0094	9.59
5	7/7/2016 9:14	7/7/2016 11:23	129	0.32	0.36	0.68	0.0052	40.61
6	7/13/2016 9:47	7/13/2016 11:09	82	0.24	0.34	0.58	0.0071	34.82
7	7/13/2016 13:46	7/13/2016 15:48	122	0.13	0.17	0.30	0.0025	18.23
8	8/25/2016 7:08	8/25/2016 9:13	125	0.22	0.44	0.66	0.0053	39.42
9	8/31/2016 12:18	8/31/2016 13:20	62	0.29	0.55	0.84	0.0136	50.44
10	9/14/2016 5:58	9/14/2016 6:43	45	0.06	0.16	0.22	0.0049	13.25
11	9/14/2016 8:16	9/14/2016 8:58	42	0.11	0.16	0.27	0.0064	16.20
12	9/14/2016 9:57	9/14/2016 10:35	38	0.10	0.12	0.23	0.0059	13.54
13	9/14/2016 10:37	9/14/2016 11:23	46	0.12	0.15	0.27	0.0059	16.32
14	9/14/2016 11:27	9/14/2016 11:57	30	0.06	0.17	0.24	0.0078	14.11
15	9/24/2016 22:52	9/24/2016 23:53	61	0.16	0.18	0.34	0.0055	20.30
16	10/4/2016 22:44	10/4/2016 23:07	23	0.02	0.13	0.14	0.0062	8.54
17	6/15/2017 0:00	6/16/2017 0:00	1440	2.88	3.83	6.72	0.0047	403.05
18	6/17/2017 0:32	6/17/2017 15:22	890	71.75	15.04	86.79	0.0975	5207.33
19	6/17/2017 0:00	6/18/2017 0:00	1440	15.78	5.02	20.80	0.0144	1248.09
20	6/18/2017 1:09	6/18/2017 4:35	206	2.20	3.43	5.63	0.0273	337.94
21	6/29/2017 6:04	6/29/2017 8:59	175	6.03	3.77	9.80	0.0560	588.11
22	6/29/2017 9:05	6/29/2017 10:46	101	1.67	1.70	3.36	0.0333	201.87
23	6/30/2017 2:56	6/30/2017 5:55	179	1.96	1.44	3.40	0.0190	204.05
24	8/21/2017 0:00	8/22/2017 0:00	1440	54.25	10.04	64.29	0.0446	3857.61
25	8/22/2017 9:08	8/22/2017 10:42	94	2.07	2.45	4.52	0.0481	271.10
26	8/27/2017 9:09	8/27/2017 12:18	189	0.25	0.26	0.51	0.0027	30.70
27	10/21/2017 0:00	10/22/2017 0:00	1440	21.91	8.39	30.30	0.0210	1818.05
28	6/11/2018 0:00	6/12/2018 0:00	1440	0.13	0.37	0.50	0.0003	29.94

8.2 Appendix 2: Base flow separation techniques

Example of hydrograph separation based on recession analysis that did not work.

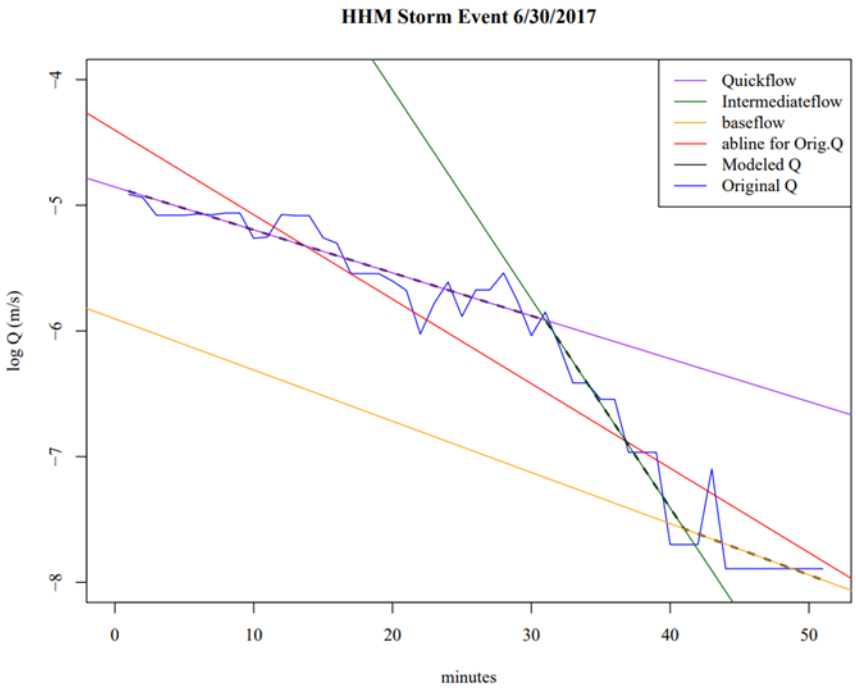

Figure 1. Recession curve of discharge (blue line) log-transformed *(Q) vs.* time with three streamflow components approximated using the linear regression form of eq. (1) and the concepts of Figure 5 in text. However, this is

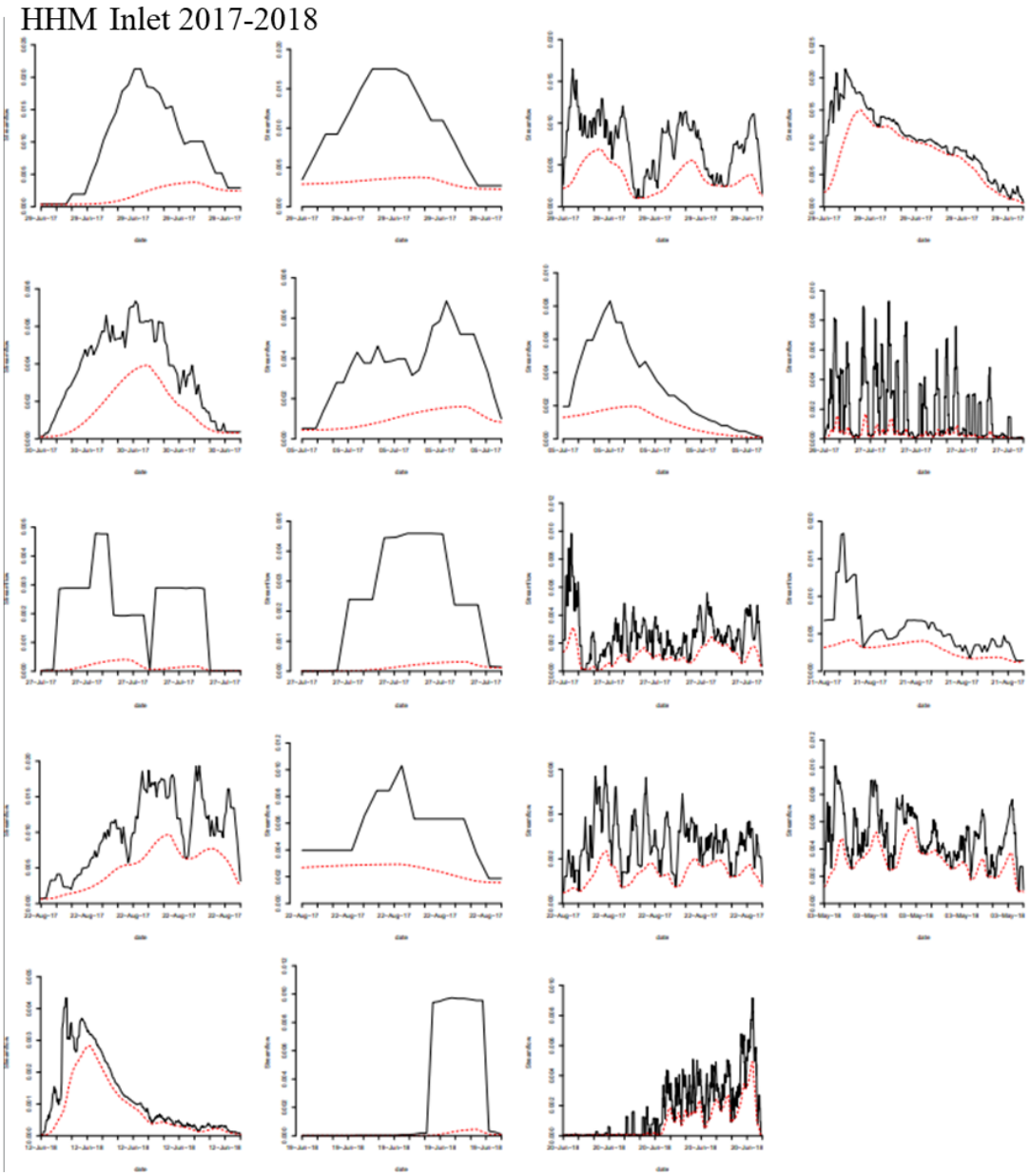

Figure 2. HHM inlet hydrographs where total discharge (Q, black) is separated using the recursive digital filter model into baseflow (red-dotted line) and the area in between is the quickflow response.

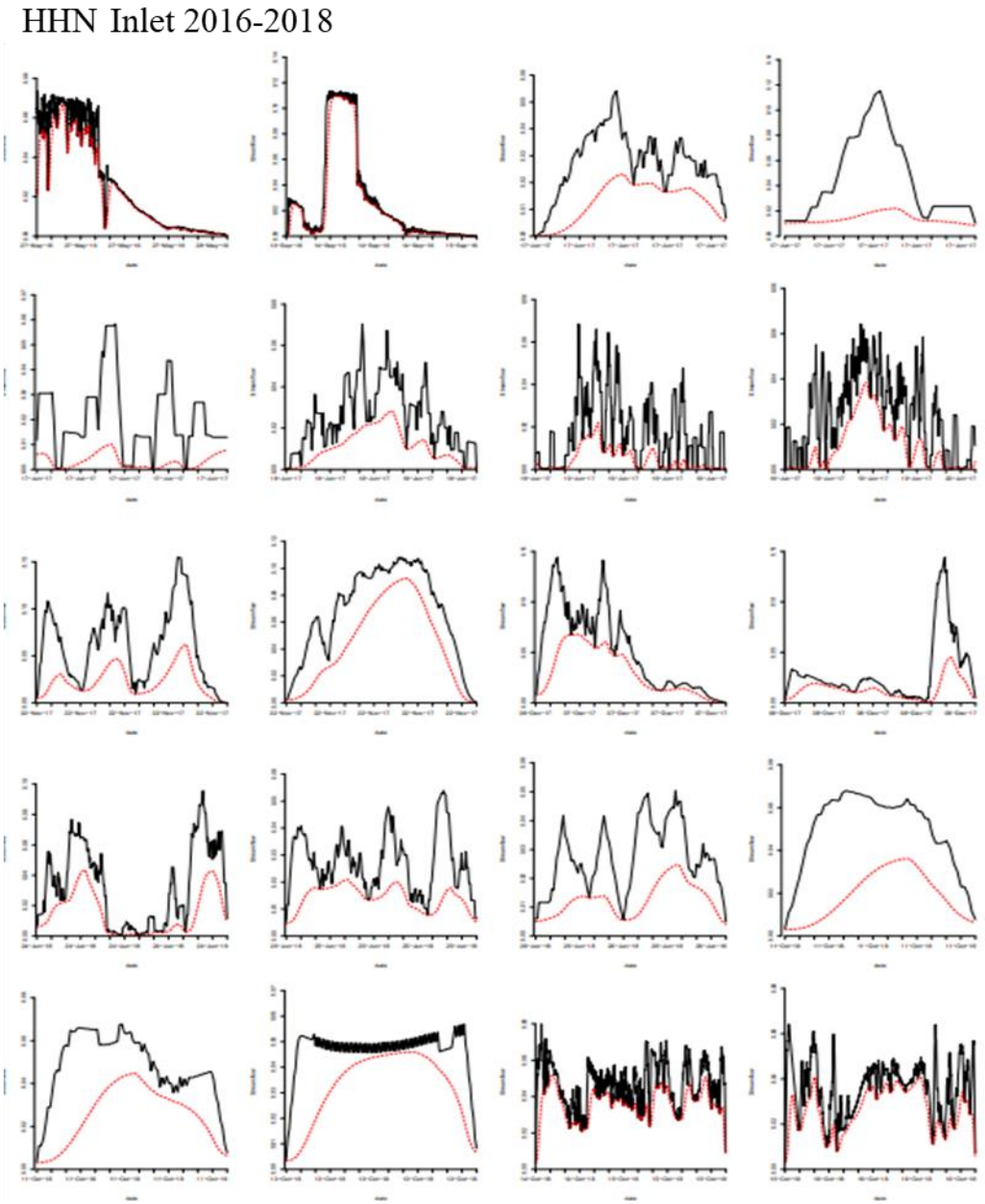

Figure 3. HHN inlet hydrographs where total discharge (Q, black) is separated using the recursive digital filter model into baseflow (red-dotted line) and the area in between is the quickflow response.

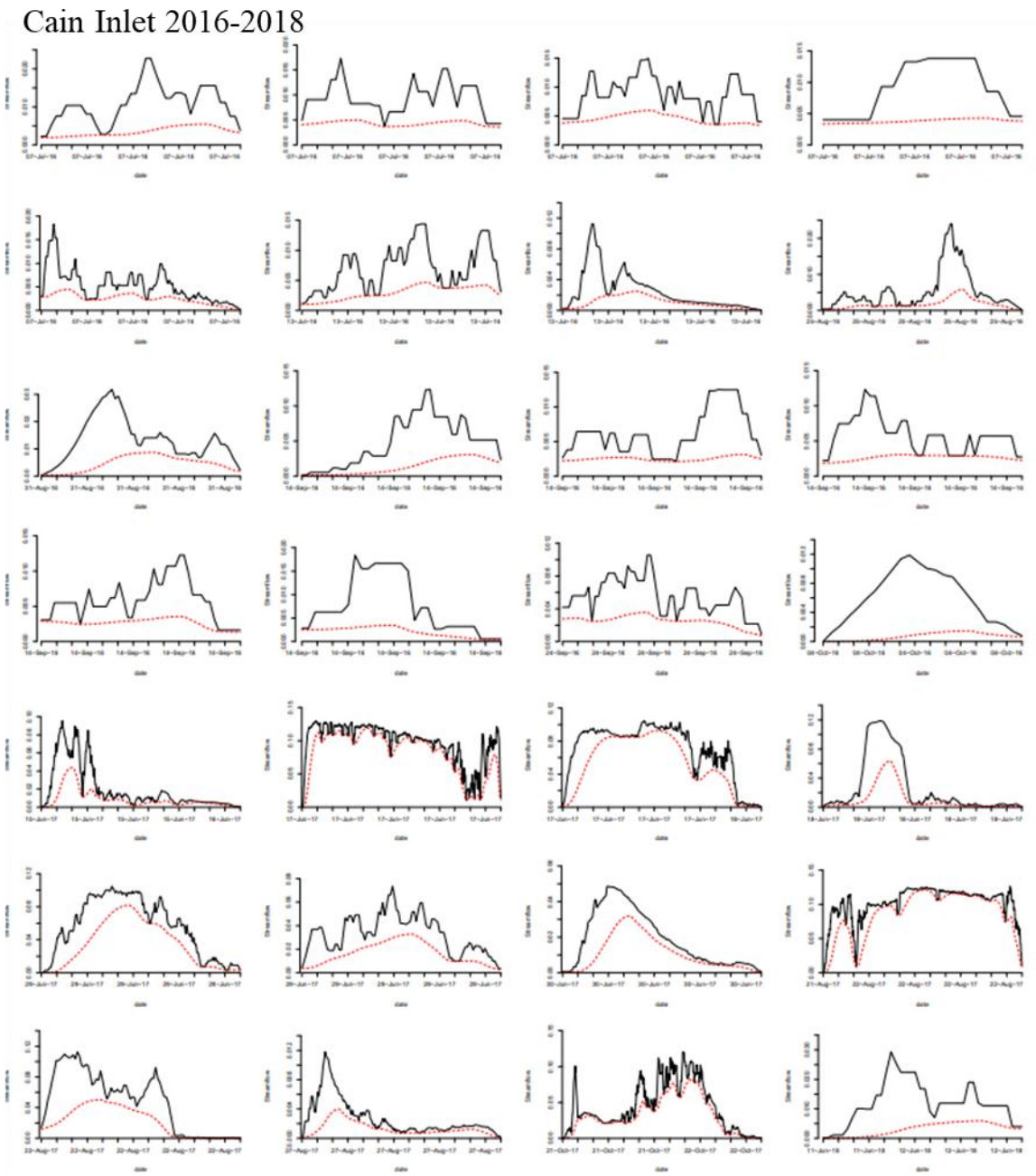

Figure 4. Cain inlet hydrographs where total discharge (Q, black) is separated using the recursive digital filter model into baseflow (red-dotted line) and the area in between is the quickflow response.

8.3 Appendix 3: Concentration Discharge Behavior

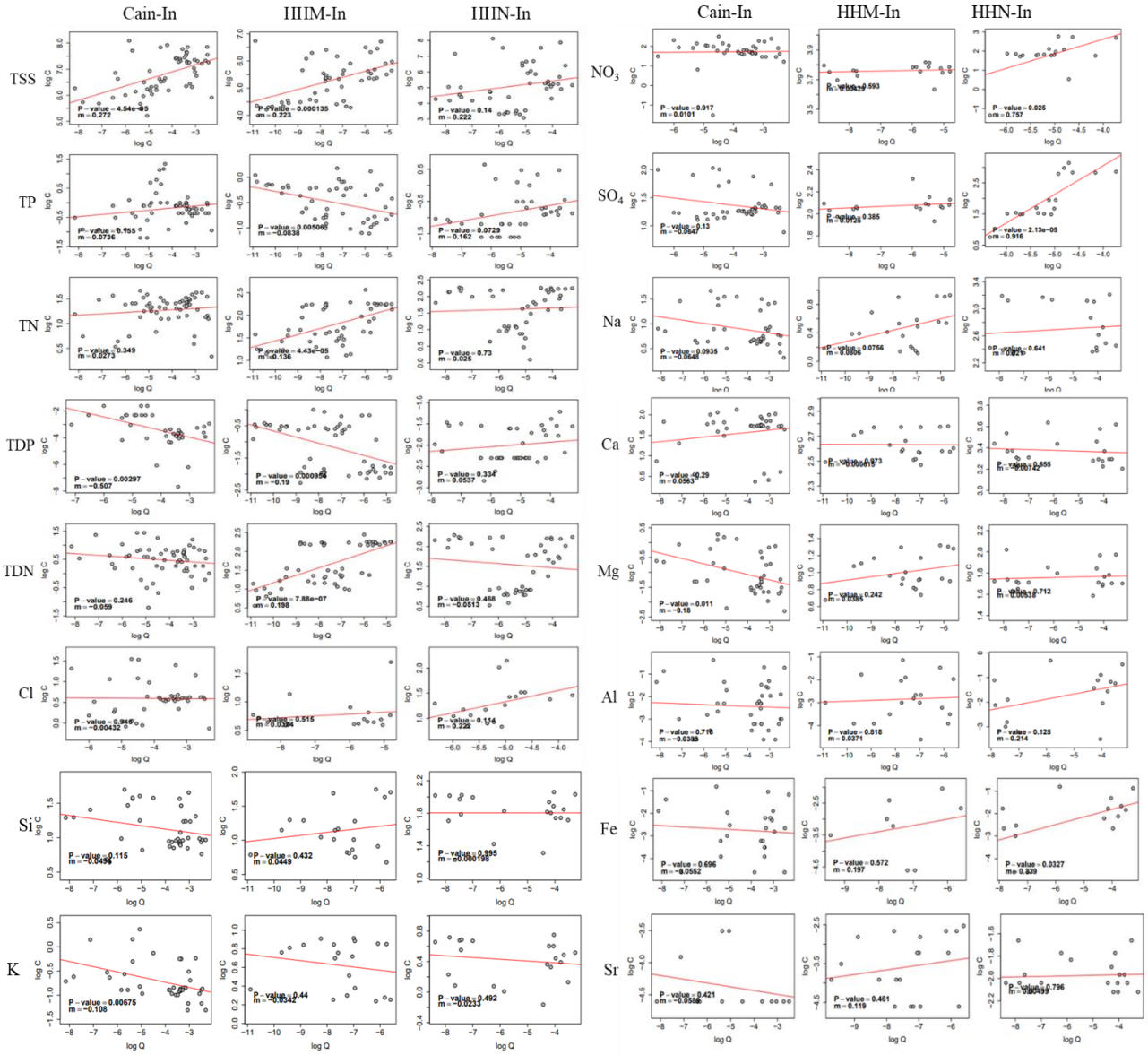

Figure 5. Concentration-discharge (C-Q) relationship of total suspended solids (TSS, mg/L), total phosphorus (TP, mg/L), total nitrogen (TN, mg/L). total dissolved phosphorus (TDP, mg/L), total dissolved nitrogen (TDN, mg/L), chloride (Cl, mg/L), silica (Si, mg/L), potassium (K, mg/L), nitrate (NO_3, mg/L), sulfate (SO_4, mg/L), sodium (Na, mg/L), calcium (Ca, mg/L), magnesium (Mg, mg/L), aluminum (Al, mg/L), iron (Fe, mg/L), and strontium (Sr, mg/L) for Cain, HHM, and HHN sites 2016-2017. Red lines depict the relationship of concentrations vs. discharge regressions with a p-value and the slope factor (m).